Quantitative interpretation of atmospheric carbon records over the last glacial termination

Peter Köhler and Hubertus Fischer

Alfred Wegener Institute for Polar and Marine Research, Bremerhaven, Germany

Guy Munhoven

Laboratoire de Physique Atmosphérique et Planétaire, Institut d'Astrophysique et de Géophysique, Université de Liège, Liege, Belgium

Richard E. Zeebe[1]

Alfred Wegener Institute for Polar and Marine Research, Bremerhaven, Germany

[1] The glacial/interglacial rise in atmospheric pCO_2 is one of the best known changes in paleoclimate research, yet the cause for it is still unknown. Forcing the coupled ocean-atmosphere-biosphere box model of the global carbon cycle BICYCLE with proxy data over the last glacial termination, we are able to quantitatively reproduce transient variations in pCO_2 and its isotopic signatures ($\delta^{13}C$, $\Delta^{14}C$) observed in natural climate archives. The sensitivity of the Box model of the Isotopic Carbon cYCLE (BICYCLE) to high or low latitudinal changes is comparable to other multibox models or more complex ocean carbon cycle models, respectively. The processes considered here ranked by their contribution to the glacial/interglacial rise in pCO_2 in decreasing order are: the rise in Southern Ocean vertical mixing rates (>30 ppmv), decreases in alkalinity and carbon inventories (>30 ppmv), the reduction of the biological pump (~20 ppmv), the rise in ocean temperatures (15–20 ppmv), the resumption of ocean circulation (15–20 ppmv), and coral reef growth (<5 ppmv). The regrowth of the terrestrial biosphere, sea level rise and the increase in gas exchange through reduced sea ice cover operate in the opposite direction, decreasing pCO_2 during Termination I by ~30 ppmv. According to our model the sequence of events during Termination I might have been the following: a reduction of aeolian iron fertilization in the Southern Ocean together with a breakdown in Southern Ocean stratification, the latter caused by rapid sea ice retreat, trigger the onset of the pCO_2 increase. After these events the reduced North Atlantic Deep Water (NADW) formation during the Heinrich 1 event and the subsequent resumption of ocean circulation at the beginning of the Bølling-Allerød warm interval are the main processes determining the atmospheric carbon records in the subsequent time period of Termination I. We further deduce that a complete shutdown of the NADW formation during the Younger Dryas was very unlikely. Changes in ocean temperature and the terrestrial carbon storage are the dominant processes explaining atmospheric $\delta^{13}C$ after the Bølling-Allerød warm interval.

Citation: Köhler, P., H. Fischer, G. Munhoven, and R. E. Zeebe (2005), Quantitative interpretation of atmospheric carbon records over the last glacial termination, *Global Biogeochem. Cycles*, *19*, GB4020, doi:10.1029/2004GB002345.

1. Introduction

[2] One crucial question of paleoclimate research still unanswered is the conceptual and quantitative understanding of glacial/interglacial (G/IG) changes in atmospheric pCO_2. During the transition from the Last Glacial Maximum (LGM) 23–19 kyr before present (BP) to the beginning of the Holocene around 11 kyr BP, measurements in ice cores reveal an increase of about 80 parts per million by volume (ppmv) [*Barnola et al.*, 1987; *Fischer et al.*, 1999; *Monnin et al.*, 2001]. Theories proposed in the past (see reviews by *Archer et al.* [2000a] and *Sigman and Boyle* [2000]) have focused on the intensities or specific aspects of either the physical or the biological pump which transport carbon from the surface to the deep ocean.

[3] Variations in the physical pump by large changes in vertical ocean mixing [*Toggweiler*, 1999], the strength of

[1]Now at the Department of Oceanography, University of Hawaii at Manoa, Honolulu, Hawaii, USA.
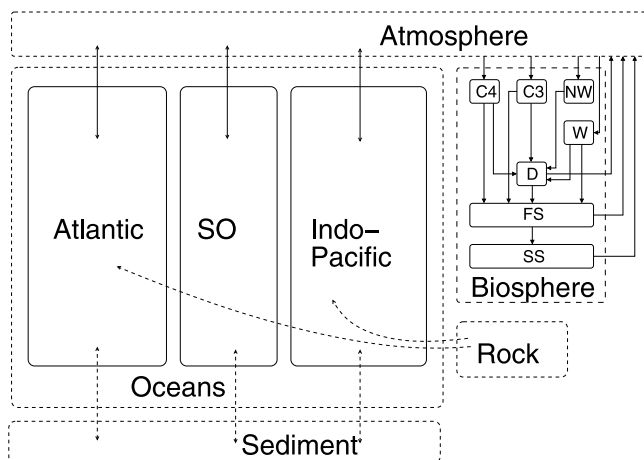
Figure 1. Geometry of the Box model of the Isotopic Carbon cYCLE (BICYCLE). Carbon fluxes between different reservoirs are shown. SO, Southern Ocean. Biosphere compartments: C4, C_4 ground vegetation; C3, C_3 ground vegetation; NW, non-woody parts of trees; W, woody parts of trees; D, detritus; FS, fast decomposing soil; SS, slow decomposing soil.

the thermohaline circulation (THC) [*Heinze et al.*, 1991], or sea ice cover limiting gas exchange rates [*Stephens and Keeling*, 2000] result in pCO_2 variations in the atmosphere. Iron fertilization in high nitrate low chlorophyll (HNLC) areas was put forward as a process acting on the biological pump which reduces pCO_2 in the LGM via increased marine export production [*Martin*, 1990; *Watson et al.*, 2000; *Ridgwell and Watson*, 2002; *Bopp et al.*, 2003; *Ridgwell*, 2003b]. The rain ratio of organic matter to calcium carbonate ($CaCO_3$) connects the two main export processes of the biological pump. Changes in the rain ratio on G/IG timescales were proposed as a hypothesis to explain observed variations in atmospheric pCO_2 [*Archer and Maier-Reimer*, 1994]. While there is nowadays evidence that the rain ratio has remained fairly constant [*Sigman et al.*, 1998; *Klaas and Archer*, 2002; *Ridgwell*, 2003a], rain ratio changes in relation to Southern Ocean processes as a potentially viable explanation for lower glacial pCO_2 have recently been discussed [e.g., *Matsumoto et al.*, 2002]. Additionally, inventories of dissolved inorganic carbon (DIC) and alkalinity (ALK) in the ocean are perturbed by fluxes of carbonate (CO_3^{2-}) and bicarbonate (HCO_3^-) in and out of the ocean via continental weathering [*Munhoven*, 2002; *Amiotte-Suchet et al.*, 2003], shallow water carbonate production through coral reef growth [*Berger*, 1982; *Opdyke and Walker*, 1992; *Vecsei and Berger*, 2004] and dissolution and sedimentation in the deep ocean [e.g., *Berger*, 1968; *Berger and Keir*, 1984; *Broecker and Takahashi*, 1978; *Crowley*, 1983; *Peterson and Prell*, 1985; *Curry and Lohmann*, 1986; *Broecker and Peng*, 1987; *Farrell and Prell*, 1989; *Archer*, 1991; *Milliman*, 1993; *Howard and Prell*, 1994; *Zeebe and Westbroek*, 2003]. The first conceptual ocean carbon cycle box models proposed either variations in the ocean circulation and high latitude mixing rates or enhanced glacial high latitude

nutrient utilization invoking greater marine biological productivity as main drivers for the G/IG rise in pCO_2 [*Knox and McElroy*, 1984; *Sarmiento and Toggweiler*, 1984; *Siegenthaler and Wenk*, 1984]. In various studies, the Southern Ocean was identified as a key area where major variations in the global carbon cycle and climate system were initiated leading to the G/IG transitions [*Toggweiler and Sarmiento*, 1985; *Sigman and Boyle*, 2000; *Stephens and Keeling*, 2000; *Knorr and Lohmann*, 2003].

[4] In this study we use for the first time a transient modeling approach to disentangle these effects which act at different times during the transition and to propose for the first time a consistent picture to explain both changes in atmospheric pCO_2 and its stable isotopic signature $\delta^{13}C$ over time. Our results are also in line with the atmospheric $\Delta^{14}C$ record and observations of $\delta^{13}C$ in deep sea sediments. To this end we force our simple ocean-atmosphere-biosphere box model forward in time, using the temporal information on boundary conditions of the global carbon cycle as revealed by proxy records in ice and sediment cores. We intentionally use a simple model which is sufficiently constrained by those boundary conditions. We concentrate on the last transition for which all data relevant for our study are available.

2. Model Description

[5] We use our Box model of the Isotopic Carbon cYCLE (BICYCLE) (Figure 1) consisting of a modified version of a globally averaged box model of the terrestrial biosphere [*Emanuel et al.*, 1984] recently applied on glacial timescales (for details, see *Köhler and Fischer* [2004]) coupled to an updated version of a multibox model of the ocean/atmosphere subsystem [*Munhoven and François*, 1996; *Munhoven*, 1997]. While the atmosphere consists of one well mixed box only, the global oceans are resolved by 10 homogeneous reservoirs (five surface, two intermediate, three deep, Figure 2). The ocean model is comparable to well tested models such as PANDORA (10 ocean boxes) [*Broecker and Peng*, 1986] or CYCLOPS (14 ocean boxes) [*Keir*, 1988]. The terrestrial biosphere is considered globally averaged by seven compartments representing C_3 and C_4 ground vegetation, trees, and soil carbon with different turnover times. Alternatively, any assumed change in the terrestrial carbon stocks or the output of more sophisticated dynamic global vegetation models (DGVM) can be applied as additional boundary conditions. The geometry of the oceanic reservoirs is based upon realistic bathymetric profiles and changes as a function of the prescribed sea level evolution. The model includes mass balance equations for the carbon stocks of the biospheric compartments, for DIC, total alkalinity, phosphate (chosen as the limiting macronutrient) and oxygen in the 10 oceanic reservoirs, for CO_2 in the atmospheric reservoir, and the ^{13}C and ^{14}C isotopic signatures in all of them. The mass balance equations include terms to represent the air-sea exchange of CO_2 and the transport of dissolved species by water circulation. Further taken into account is the production of organic and inorganic (carbonate) particles by marine biological activity in the surface layer. Organic particles and inorganic carbonate
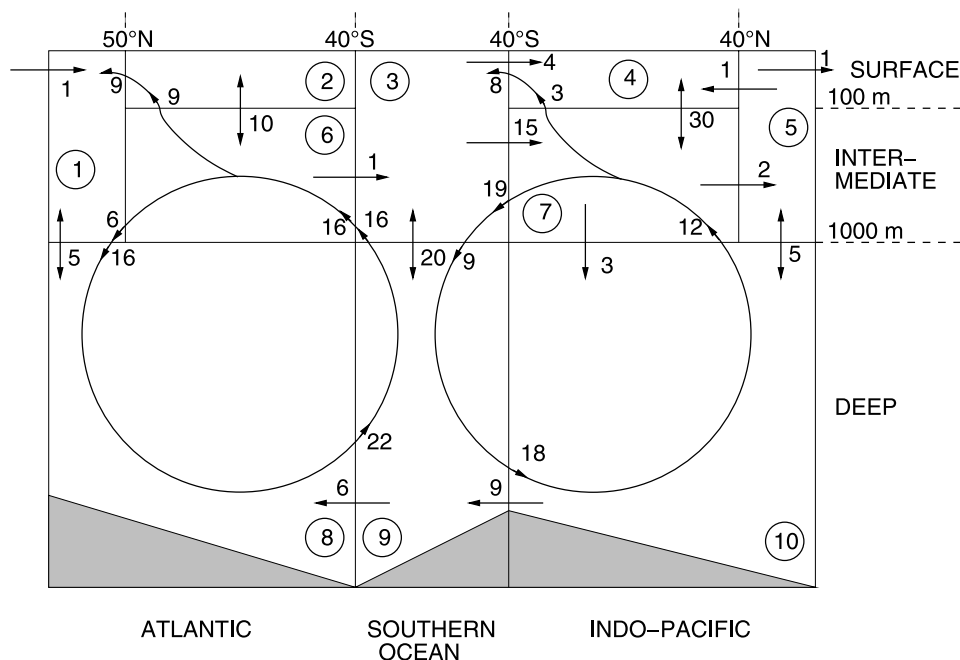
Figure 2. Geometry of the ocean box model and recent fluxes of ocean circulation (in Sv = 10^6 m^3 s^{-1}). Box numbers are given in circles.

rain down to the intermediate and deep reservoirs where they are remineralized or deposited.

3. Preindustrial Parameter Setting

[6] The original ocean-atmosphere model [*Munhoven*, 1997] is updated in various ways. We used C:N:P:O$_2$ = 123:17:1:−165 as elemental (Redfield) ratios during marine production and remineralization [*Körtzinger et al.*, 2001]. The chemical equilibrium of the oceanic carbonate system is based on a recent review [*Zeebe and Wolf-Gladrow*, 2001] with updates of the dissociation constants pK$_1$ and pK$_2$ [*Prieto and Millero*, 2002]. Recent ocean temperature and salinity are prescribed from data based on the World Ocean Atlas [*Levitus and Boyer*, 1994b; *Levitus et al.*, 1994].

[7] Mean annual sea ice covers of the Arctic and Southern Ocean surface boxes (10 × 10^{12} m^2 each) are realized by reducing gas exchange rates relative to areal ice cover based on current knowledge on recent sea ice extents [*Cavalieri et al.*, 1997; *Vinnikov et al.*, 1999; *Fichefet et al.*, 2003].

[8] The ocean-atmosphere gas exchange is a function of temperature via the solubility of CO$_2$ and piston velocity (2.5 and 7.5 × 10^{-5} m s^{-1} for low and high latitudes, respectively) which is based on wind speed to resolve latitudinal differences [*Heimann and Monfray*, 1989; *Sarmiento et al.*, 1992; *Wanninkhof*, 1992]. The average gas exchange coefficient (0.051 mol m^{-2} yr^{-1} μatm^{-1}) is of the same order as in ^{13}C/^{12}C studies [*Heimann and Maier-Reimer*, 1996] and leads to a preindustrial gross flux of CO$_2$ between ocean surface and atmosphere of about 60 PgC yr^{-1}.

[9] The isotopic fractionation during the gas exchange is a function of temperature [*Zhang et al.*, 1995]. The fractionation during marine organic production follows a

temperature and CO$_2$ (aq) dependent scheme [*Rau et al.*, 1996, 1997; *Ridgwell*, 2001], while for inorganic CaCO$_3$ production a simple temperature-dependent fractionation is assumed [*Mook*, 1986].

[10] Ocean circulation and especially recent deep water production (DWP) is based on WOCE data [*Ganachaud and Wunsch*, 2000]. We use 16 Sv (1 Sv = 10^6 m^3 s^{-1}) of North Atlantic Deep Water (NADW) formation and 9 Sv for the effective production of Antarctic Bottom Water (AABW) (Figure 2). The latter results from the difference between 21 ± 6 Sv downwelling and 8 ± 9 Sv upwelling in the Southern Ocean as estimated by *Ganachaud and Wunsch* [2000]. The missing DWP of AABW is matched by the vertical mixing fluxes. Data suggest equatorial mixing between surface and intermediate boxes (20 Sv Atlantic, 60 Sv Indo-Pacific [*McPhaden and Zang*, 2002] which is driven by equatorial upwelling, Ekman pumping [*Wunsch*, 1984] and subduction [*Qiu and Huang*, 1995]. The vertical exchange in high latitudes (60 Sv) mainly occurs in the Indo-Pacific section of the Southern Ocean [*Sloyan and Rintoul*, 2001]. To obtain best agreements between the steady state global behavior of the oceanic module for preindustrial conditions with observations (DIC, alkalinity and GLobal Ocean Data Analysis Project GLO-DAP at http://ferret.pmel.noaa.gov/GLODAP [*Takahashi et al.*, 1981; *Millero et al.*, 1998; *Key et al.*, 2004], PO$_4$ [*Conkright et al.*, 1994], O$_2$ [*Levitus and Boyer*, 1994a], δ^{13}C [*Kroopnick*, 1985], Δ^{14}C [*Stuiver et al.*, 1981]) we had to revise original vertical mixing strengths and divided them by a factor of 2. This discrepancy is attributed to our coarse ocean model resolution especially in the vertical direction and brings our ocean circulation pattern closer to other box model studies [e.g., *Broecker and Peng*, 1986; *Keir*, 1988]. Southern Ocean vertical mixing assumed here (20 Sv) is

Table 1. Ocean Settings for the Preindustrial Reference Run[a]

Number	Name	Area, $10^{12}m^2$	Volume, $10^{15}m^3$	Temp,[b] °C	Sal[c]	τ,[d] years	PO$_4$	O$_2$	ALK	DIC	$[CO_3^{2-}]$	pCO$_2$, ppmv	pH	δ^{13}C, ‰	Δ^{14}C, ‰
						Surface Boxes									
1	North Atlantic	20	12	2.4	34.6	19	0.55	328	2308	2092	154	234	8.21	1.56	−64
2	Eq. Atlantic	65	6	20.7	36.1	11	0.15	221	2326	1971	254	268	8.18	1.76	−61
3	Southern Ocean	76	74	4.6	34.5	35	1.37	312	2349	2140	152	270	8.16	1.40	−77
4	Eq. Indo-Pacific	182	18	23.2	35.0	15	0.11	212	2352	1976	272	267	8.18	1.42	−76
5	North Pacific	15	13	4.2	33.9	59	1.99	316	2374	2167	152	275	8.16	1.57	−86
						Intermediate Boxes									
6	Eq. Atlantic		55	9.7	35.2	67	1.72	140	2328	2177	117		7.93	0.76	−78
7	Eq. Indo-Pacific		156	9.5	34.7	87	1.77	78	2350	2196	122		7.96	0.42	−108
						Deep Boxes									
8	Atlantic		204	2.9	34.9	239	1.52	181	2333	2211	94		7.87	0.66	−101
9	Southern Ocean		218	1.3	34.7	109	1.94	173	2353	2234	92		7.89	0.57	−112
10	Indo-Pacific		585	2.2	34.7	713	2.70	62	2389	2332	63		7.69	0.10	−176
	Whole ocean	358	1341	3.8	34.7	382	2.10	125	2363	2253			7.83	0.44	−133
	Atmosphere											267		−6.55	−6

[a]Weathering flux and ocean/sediment exchange off. C_{exp} = 10 PgC yr^{-1}, C_{exp}:CaCO$_3$ = 10, both at 100 m water depth. Unit of measure is μmol kg^{-1} for PO$_4$, O$_2$, ALK, DIC, and $[CO_3^{2-}]$.
[b]Prescribed from WOA [*Levitus and Boyer*, 1994b].
[c]Prescribed from WOA [*Levitus et al.*, 1994].
[d]Turnover time.

thus also of the order of magnitude estimated recently (14 Sv) by a study which applied "residual mean theory" to transient tracer uptake [*Ito et al.*, 2004]. Thus, especially, box turnover times and Δ^{14}C (Table 1) are now in line with observations [*Stuiver et al.*, 1981], which find a Δ^{14}C of −50‰ to −100‰ in surface waters and −80‰ to −200‰ in the deep ocean. In our preindustrial reference scenario, deep Indo-Pacific waters are mostly of NADW origin. The age of these deep Indo-Pacific waters calculated with the box turnover times and consideration of the water transport as depicted in Figure 2 is estimated to more than 900 years. The recent ^{14}C production rate is set to 450 mol yr^{-1} to match radiocarbon decay rates and to allow our simulations to start from steady state, and is thus lower than the widely used estimate of *Masarik and Beer* [1999].

[11] The preindustrial flux of export production of organic matter from the surface to the deep ocean is prescribed at 100 m water depth with 10 PgC yr^{-1} [*Schlitzer*, 2000; *Gnanadesikan et al.*, 2002; *Sarmiento et al.*, 2002]. (Note that Southern Ocean export was not prescribed during transient model runs; compare section 5.3). We assume a constant rain ratio between organic and CaCO$_3$ production of 10 [*Sigman and Boyle*, 2000; *Harvey*, 2001; *Koeve*, 2002; *Sarmiento et al.*, 2002; *Schiebel*, 2002]. Data and modeling constraints on the spatial distribution of the export production find about two thirds of the global export flux in equatorial regions (and there in the coastal upwelling zones), a fourth in the Southern Ocean, 10–20% in the North Atlantic and very little in the Northern Pacific [*Schlitzer*, 2000, 2002; *Gnanadesikan et al.*, 2002]. To account for these regional differences in marine production all macro-nutrients in the equatorial regions are utilized for export (4.4 PgC yr^{-1}), whereas the missing amount of carbon export to reach the proposed global production of 10 PgC yr^{-1} is supplied by prescribed fluxes in the three high latitudinal areas (North Atlantic: 1.6 PgC yr^{-1}); Southern Ocean: 3.4 PgC yr^{-1}; North Pacific: 0.6 PgC yr^{-1}).

Since the large nutrient gradients in the equatorial regions are not resolved in our study, the export production in our model compared with other studies is higher in the Southern Ocean and lower in the equatorial boxes, but consistent with a previous box model study [*Sigman et al.*, 1998]. From the marine biological production in the surface layers, 18% of the organic material and 80% of CaCO$_3$ reach the deep ocean below 1000 m depth. If the O$_2$ concentration drops below 4 μmol kg^{-1} the remineralization of organic matter in the deep ocean is assumed to follow the denitrification pathway and thus does not consume any molecular oxygen. This is in line with the Ocean Carbon-Cycle Model Intercomparison Project (OCMIP) 2 protocol and field data on zooplankton abundance [*Saltzman and Wishner*, 1997]. While anoxic conditions do not occur for preindustrial model conditions, they do occur during time-dependent model scenarios when large changes in oceanic overturning are assumed (to be investigated later on).

[12] In our steady state result of the reference run for the preindustrial climate (Table 1), atmospheric pCO$_2$ settles at 267 ppmv. The Δ^{14}C of the ocean boxes as a proxy for model turnover times fall within the ranges observed by *Stuiver et al.* [1981] with the exception of the deep Southern Ocean where Δ^{14}C is about 20‰ too heavy.

4. Model Evaluation and Sensitivities

[13] There is an ongoing discussion about the sensitivities of ocean carbon cycle models of various complexity to changes in either the low or the high latitudinal surface ocean [*Broecker et al.*, 1999; *Archer et al.*, 2000b; *Toggweiler et al.*, 2003a, 2003b] (see also R. E. Zeebe, Simple ocean carbon cycle models: New insights into evaluating glacial CO$_2$ scenarios and predictions of anthropogenic CO$_2$ uptake by the ocean, submitted to *Global Biogeochemical Cycles*, 2005) (hereinafter referred to as Zeebe, submitted manuscript, 2005). Thus it was shown that atmospheric pCO$_2$ calculated
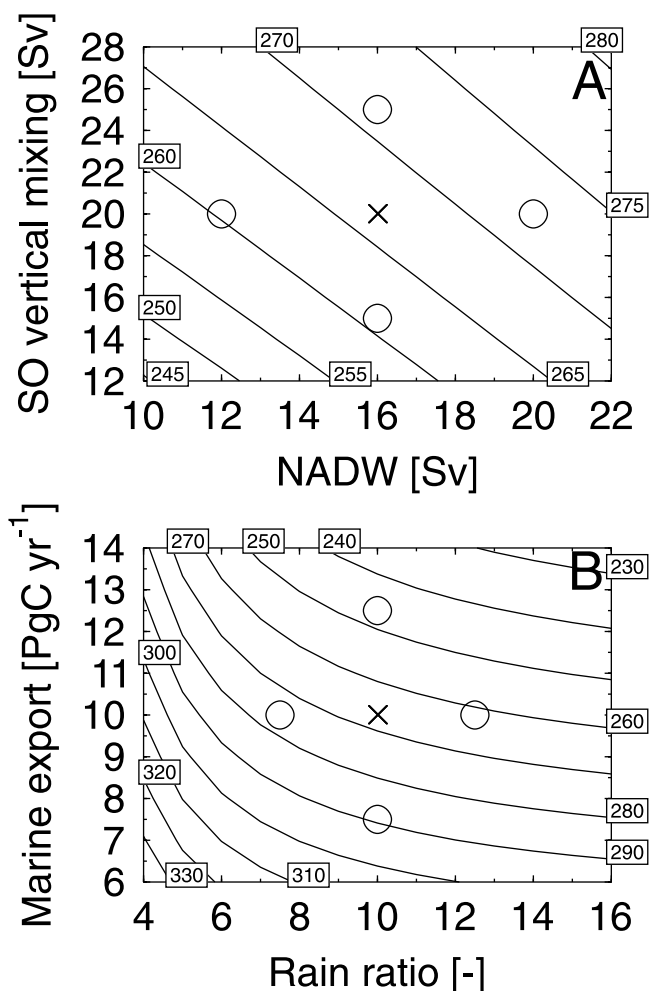
Figure 3. Contours of atmospheric pCO_2 and its sensitivity to various parameters. (a) Variations in the ocean circulation (strength of NADW formation and Southern Ocean vertical mixing rate). (b) Variations in the biological pump (global marine export production and rain ratio of organic carbon to $CaCO_3$). Crosses mark the pCO_2 of our preindustrial reference run; circles mark variations of 25% in one parameter.

with simple box models have a high sensitivity to variations in the high latitudes, while pCO_2 derived from multibox models and particularly GCMs is more sensitive to changes in the low-latitude oceans.

[14] We perform two tests regarding the sensitivity of BICYCLE in the context of other carbon cycle models. First, the model-calculated pCO_2 derived by an "abiotic" ocean is determined to evaluate its high latitudinal sensitivity. This abiotic test is performed by setting marine export fluxes of both organic and inorganic material to zero. The lower the final atmospheric pCO_2 of the model, the larger is its high-latitude sensitivity, because of higher solubility of pCO_2 in colder surface water. The test was first applied by *Archer et al.* [2000b] to a variety of different models and extended recently (Zeebe, submitted manuscript, 2005). We use the same initialization of the carbonate system to allow

comparison with these studies (ALK = 2371 μmol kg^{-1}, DIC = 2085 μmol kg^{-1}, atmospheric pCO_2 = 278 ppmv). In this setting, BICYCLE has an abiotic pCO_2 of 221 ppmv, which is in the range of CYCLOPS (pCO_2 = 221 ppmv) and PANDORA (pCO_2 = 230 ppmv), but lower than most more complex ocean carbon cycle models.

[15] In a second test, the low-latitude sensitivity of the ocean/atmosphere component is tested by calculating the Harvardton Bear Equilibration Index (HBEI) [*Broecker et al.*, 1999]. The HBEI is calculated by a perturbation of the solubility of CO_2 in the warm equatorial surface ocean. It varies between 0 and 1 and is a measure for the modeled sensitivity of atmospheric pCO_2 to changes in the warm low latitudinal surface ocean. HBEI can either be calculated for the perturbations of atmospheric pCO_2 or using the warm surface ocean's partial pressure. Typical values are 0.1 for three-box ocean models to 0.3–0.4 for 3D GCMs. As already mentioned [*Broecker et al.*, 1999], the HBEI varies with the strength of the perturbation, but converges with decreasing solubility to stable values. Here the HBEI of the average warm surface ocean is 0.39 for a decrease in CO_2 solubility by 30%, and converges to 0.30 for smaller values. Thus BICYCLE is more sensitive to changes in the warm oceans than CYCLOPS (HBEI = 0.19) or PANDORA (HBEI = 0.22) and is close to the warm water sensitivity of 3D GCMs (0.24–0.32). One has to note that the definition of warm equatorial waters here is slightly different from that of *Broecker et al.* [1999], who used 40°S–40°N, while our Atlantic equatorial box reaches as far north as 50°N. Taken together, the model sensitivity of the ocean module in BICYCLE, at least of its physical system, is in the range of other multibox models.

[16] To elucidate the model sensitivity to important parameters, we perform some two-dimensional parameter variations (Figure 3). The atmospheric pCO_2 is remarkably stable in response to small changes in ocean circulation (Figure 3a). A change in NADW formation or Southern Ocean vertical mixing by 25% would, for example, alter pCO_2 by 5 ppmv only. The model is more sensitive to variations in the biological pump (Figure 3b). Increasing or decreasing marine export production by 25% alters atmospheric pCO_2 by more than 20 ppmv. On the other hand, the model is a factor four less sensitive to changes in the rain ratio. Varying the rain ratio by 25% changes pCO_2 by ~5 ppmv.

[17] If we compare our ocean setting for the preindustrial reference run (Table 1) with the newest data compilation from GLODAP [*Key et al.*, 2004] and other sources [*Kroopnick*, 1985; *Conkright et al.*, 1994; *Takahashi et al.*, 2002], we find agreements with our ocean variables (DIC, ALK, PO_4, $\delta^{13}C$, $\Delta^{14}C$). DIC, ALK, and pCO_2 comparisons are depicted as examples in Figure 4. Especially, modeled DIC agrees well with the DIC corrected for anthropogenic carbon of GLODAP (Figure 4b). Modeled ALK in surface waters of the Indo-Pacific and the Southern Ocean (equatorial Atlantic) are about 50 μmol kg^{-1} higher (lower) than in GLODAP (Figure 4c). The comparison of pCO_2 with the climatology of *Takahashi et al.* [2002], which was here uniformly corrected by 82 ppmv for anthropogenic carbon to yield a similar global mean pCO_2, shows clearly that the Atlantic distribution of pCO_2
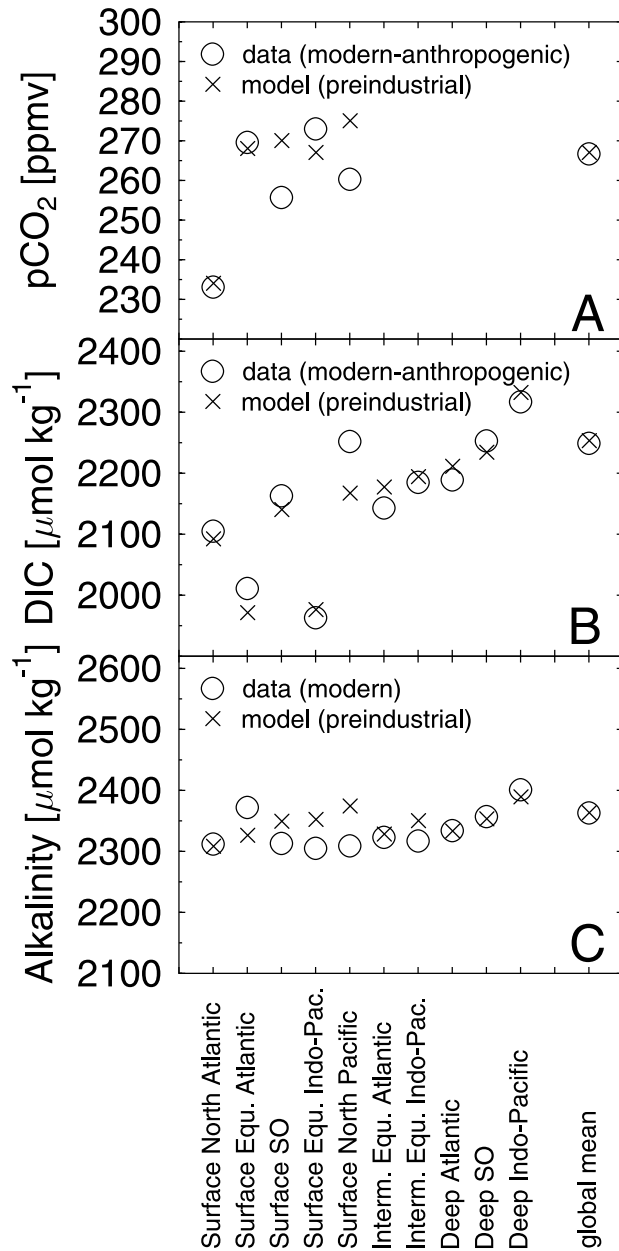
Figure 4. Comparison of (a) pCO_2, (b) DIC, and (c) alkalinity from the preindustrial reference run with data. Modern pCO_2 data from *Takahashi et al.* [2002] corrected by 82 ppmv (anthropogenic component) in order to yield the same global mean pCO_2 as in the model. DIC and alkalinity from GLODAP [*Key et al.*, 2004]. DIC data were corrected for anthropogenic carbon. See color version of this figure in the HTML.

including the North Atlantic sink is reconstructed properly by the model, while regional details of the other surface areas are only matched with an error of up to 15 ppmv (Figure 4a). We tend to underrepresent PO_4 in equatorial areas (not shown) which is caused by our low-resolution

box model, in which high nutrient concentrations found in coastal upwelling regions cannot be depicted properly. The depth gradients in the isotopic carbon records are fairly well reconstructed. Please remember that an accurate representation of $\Delta^{14}C$ was one of our criteria for model fine tuning. $\delta^{13}C$ data [*Kroopnick*, 1985] show smallest values (0.0– 0.5‰) in the deep Pacific, while in other deep ocean basins, $\delta^{13}C$ varies approximately between 0.5–1.0‰. Surface values are around 1.5–2.0‰. These distributions are all covered in our reference run.

5. Time-Dependent Changes

[18] In the following we identify the impacts of different processes on the atmospheric carbon records as summarized in Table 2. We start with short descriptions of individual processes and explain our assumptions on their implementations in the model. The temporal evolution of the carbon cycle including all these processes during Termination I will be covered in the next section. Considered here are changes in temperature, sea level, sea ice cover, ocean circulation, marine and terrestrial biosphere, weathering inputs, sediment/deep ocean exchange of alkalinity and carbon and coral reef growth. They are all first analyzed individually in the absence of any other processes such as $CaCO_3$ compensation. We will highlight how current theories on causes of G/IG changes agree or conflict with the observations. Only from the analysis of a combination of all these time-dependent processes a conceptual understanding of the underlying causes of observed changes in the carbon cycle emerges. We finally attempt to explain the temporal evolution during the course of Termination I. All transient simulations covering Termination I were spun up for 30 kyr to reach steady state, then started at t = 26 kyr BP and subsequently forced as described below using measured data sets. The long spin-up time is necessary to obtain steady states in ^{14}C.

[19] Atmospheric pCO_2 during the last termination was measured most accurately on the EPICA Dome C ice core (EDC) [*Monnin et al.*, 2001]. Data on the stable carbon isotope $\delta^{13}C$ are hitherto only available from the Taylor Dome (TD) ice core [*Smith et al.*, 1999], while $\Delta^{14}C$ data sets exist back to 15.5 kyr BP from INTCAL98 [*Stuiver et al.*, 1998] and measurements on ocean sediments from the Cariaco basin extending farther back in time [*Hughen et al.*, 2004]. These are our target records which should be interpreted in our modeling study (Figure 5).

[20] For our modeling experiment we ultimately need all proxy records on the same timescale. We have chosen to synchronize all ice core archives to the timescale of the annual layer counted Greenland GISP2 ice core [*Meese et al.*, 1997] and use the starting and end points of the three fast regime shifts in CH_4 (LGM-Bølling-Allerød (BA), BA-Younger Dryas (YD), YD-Holocene) as tie points for the synchronization of EDC and GISP2 and linearly interpolate between them. Owing to a lack of a further tie point before 15 kyr BP, the data records of EDC during the first half of the termination are shifted on the GISP2 age scale based on the LGM-BA transition only. Thus the relative timing of the records at the beginning of the

Table 2. Contribution of Different Processes on the Observed Changes in Atmospheric pCO$_2$ During Termination I (11.5–18 kyr BP)

Process	Modeled changes in pCO$_2$ (ppmv)	
	individual process	combined scenarios
Regrowth of terrestrial biosphere	−34	−20
Rise of sea level	−12	−6
Reduction of sea ice cover	−5	−2
Coral reef growth	+3	+1
Increase of the strength of NADW formation	+12	+16
Rise of ocean temperatures	+32	+17
Reduction of marine export production	+19	+22
Variations in sedimentation/dissolution and weathering rates	+7[a]	+34
Breakdown of Southern Ocean stratification	+37	+37
Summed up change	+59	+97
Simulated changes in scenario A-TB0		+87
Nonlinearities		−10

As the processes influence each other both their individual impact and the effect during combined scenarios are summarized. A comparison of the impacts of all processes in combined scenarios is only useful for closed system simulations following mass conservation. But the sediment/ocean exchange processes change the inventories of ALK and DIC. We therefore analyze the impact of single processes in combined scenarios by their exclusion from scenario A-TB0 without sediment/ocean exchange processes. The simulation of changes in DIC and ALK inventories sums up the difference between the scenarios A-TB0 with and without sediment/ocean exchange. Summed up changes differ from simulated changes because of nonlinearities of the simulated carbon cycle system.
[a]Accompanied by the growth of the terrestrial biosphere.

termination might be most uncertain, but CH$_4$ records of GISP2 and EDC are still in good agreement (Figure 6). Owing to these missing CH$_4$ tie points at the beginning of the termination and simultaneous measurements of pCO$_2$ and δ^{13}C on the TD ice core the TD δ^{13}C is best synchronized via pCO$_2$ to EDC and than to GISP2. The uncertainty in TD pCO$_2$ is 3 ppmv (2σ), which gives a synchronization uncertainty of the TD δ^{13}C of about 150 years during times of fast changes in pCO$_2$ (onset of pCO$_2$ rise and YD), 375 years during the Heinrich I event, and rather uncertain timing in periods of stable pCO$_2$ values (LGM, BA, Holocene). The main uncertainty in the dating of the ice core records is the gas age–ice age difference which increases with depth and is of the order of at least 500 years during the transition [*Monnin et al.*, 2001]. To avoid implying an unfounded phase relationship between ice and sediment records, the latter are used on their own timescale. The age uncertainty in sediment records calibrated with AMS ^{14}C is of the order of 150 years [*Visser et al.*, 2003], but highly depends on the assumed reservoir correction for ^{14}C. Data sets from highly fluctuating records were used after low-pass filtering using a 500-year running mean (see Figure 6).

5.1. Sea Level, Temperature, and Sea Ice

[21] Sea level changes deduced from coral reef terraces [*Fairbanks*, 1990] influence directly the salinity and concentrations of all oceanic tracers but also volumes and areas of the ocean boxes (Figure 6). The rise in sea level by 85 m between 20 and 10 kyr BP leads to a decrease in salinity by 2.3%. As a consequence, pCO$_2$ will fall by about 12 ppmv (6 ppmv in combined scenarios where all processes are changed simultaneously) without any relevant impact on the carbon isotopes (Figures 7a and 7b).

[22] We use the isotopic temperature proxies of the GISP2 δ^{18}O [*Grootes and Stuiver*, 1997] and EDC δD [*Jouzel et al.*, 2001] ice core records as proxies for the temporal

evolution of sea surface temperature (SST) in the northern North Atlantic and the Southern Ocean, respectively, and rescale its G/IG amplitude (ΔT = 4K) to avoid the SST below seawater freezing point [e.g., *Pflaumann et al.*, 2003; *Becquey and Gersonde*, 2003] (Figure 6). Changes in equatorial SST with a maximum amplitude of about 3.75 K are taken from observations in foraminiferal proxy records [*Visser et al.*, 2003]. This amplitude is larger than previous estimates of the G/IG rise in equatorial temperature [*CLIMAP*, 1976], but consistent with other recent studies [e.g., *Aeschbach-Hertig et al.*, 2000; *Lea et al.*, 2000; *Nürnberg et al.*, 2000; *Guilderson et al.*, 2001]. Temperature changes in the intermediate boxes follow those of the underlying deep sea boxes with G/IG amplitudes between 20 and 10 kyr BP of 1.9 to 2.4 K forced by data sets from *Labeyrie et al.* [1987], recently confirmed by *Martin et al.* [2002].

[23] Rising ocean temperatures add an increase of 32 ppmv (17 ppmv in combined scenarios, Table 2, Figure 7a). For the impact of temperature on δ^{13}C, not only changing reservoir sizes of atmospheric and oceanic carbon pools have to be considered; the fractionation during gas exchange between atmosphere and surface ocean also depends directly on temperature (Figure 7b) leading to an overall increase in δ^{13}C of 0.4‰ in the course of the transition. It might be argued that the data sets and here especially the ice core records taken as temperature proxies are not representative for the selected ocean basins. For the Southern Ocean the regional aspect of Antarctic ice core temperature was recently confirmed [*Becquey and Gersonde*, 2003], but a lag of continental Antarctic temperature and SST of the oceanic moisture source regions might exist [*Stenni et al.*, 2001]. The detailed choice of equatorial temperature proxies is of minor importance, because half of the simulated changes in pCO$_2$ are caused by Southern Ocean temperature rise, one fourth by the North Atlantic and only about one tenth by the change in SST in each of the equatorial reservoirs.
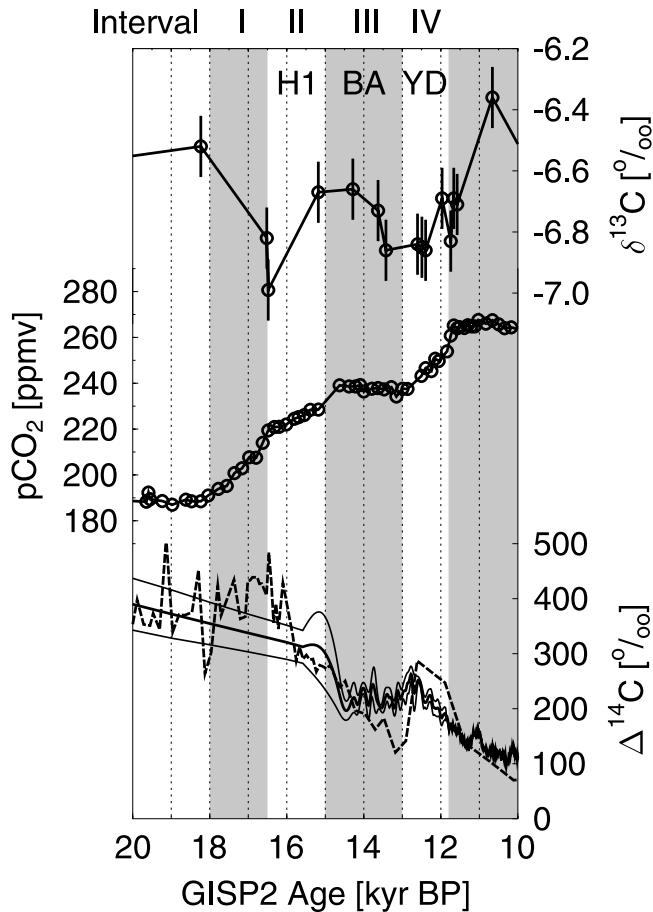
Figure 5. Measured atmospheric carbon records. Atmospheric $\delta^{13}C$ in the Taylor Dome ice core [*Smith et al.*, 1999]; pCO_2 in the EPICA Dome C ice core divided in four intervals with different changing rates [*Monnin et al.*, 2001]; $\Delta^{14}C$ from INTCAL98 (solid line with error range in thin lines) [*Stuiver et al.*, 1998] and new data from the Cariaco Basin (dashed line) [*Hughen et al.*, 2004]. The intervals II, III, and IV are approximately identical with the Heinrich 1 event (H1), the Bølling-Allerød warm interval (BA), and the Younger Dryas cold event (YD) in the North Atlantic region. See color version of this figure in the HTML.

[24] New proxy studies find LGM Southern Ocean sea ice cover of approximately twice the size of today in winter and a remarkable glacial increase in the Atlantic section of the Southern Ocean in summer [*Crosta et al.*, 1998a, 1998b; *Gersonde et al.*, 2005]. In the Northern Hemisphere summer, sea ice seemed to be far more restricted than proposed previously [*CLIMAP*, 1976; *Sarnthein et al.*, 2003]. Thus we assume annual averaged sea ice areas during the LGM of 14 and 22 $\times 10^{12}$ m^2 for the Northern and Southern Hemisphere, respectively. The temporal evolution of the sea ice area is coupled to local temperature proxies of GISP2 and EDC. Its direct influence on the gas exchange rates between atmosphere and surface ocean contributes a reduction of 2–5 ppmv to the evolution of pCO_2 (Figure 7a), its amplitude depending on single or combined process analysis (Table 2).

[25] The impact of sea ice and thus gas exchange on pCO_2 is strongly model dependent [*Archer et al.*, 2003]. Furthermore, previous studies focused on the sea ice cover in the Southern Ocean [*Stephens and Keeling*, 2000; *Morales-Maqueda and Rahmstorf*, 2002], and suggested it to be a cause for the observed rise in G/IG pCO_2. We note that our data-based assumption of sea ice variations in the south (which in the preindustrial setting is a source for atmospheric CO_2) does impact only marginally on pCO_2, but the contribution from the north (a sink for CO_2) reduces pCO_2 during the transition. Here the sea ice covers increase from their preindustrial values of 50% and 13% in the North Atlantic and Southern Ocean, respectively, to 85% and 30% during the LGM. The sea ice effect is large in box models, when a surface box is nearly fully covered by sea ice and gas exchange is thus prevented. This was also the case in the study of *Stephens and Keeling* [2000].

5.2. Ocean Circulation

[26] On the basis of observational estimates and modeling studies, the North Atlantic Deep Water (NADW) formation is assumed to be reduced [*Curry et al.*, 1988; *Duplessy et al.*, 1988] by about 40% of its modern strength to 10 Sv during glacial times [*Winguth et al.*, 1999; *Meissner et al.*, 2003] and completely shut-off during Heinrich (H) events [*Alley and Clark*, 1999; *Schulz et al.*, 2001; *Rahmstorf*, 2002; *Knutti et al.*, 2004; *McManus et al.*, 2004]. In the YD cold event (approximately 13–11.8 kyr BP), NADW formation is not shut down completely, but reduced by 15% [*McManus et al.*, 2004]. The THC is resumed at the beginning of the warming into the BA [*Charles and Fairbanks*, 1992] to intermediate strength of 13 Sv, since ongoing freshwater from melting inland ice sheets to the North Atlantic still reduces the strength of NADW formation [*Knorr and Lohmann*, 2003] (Figure 6).

[27] The reduction of NADW formation by 40% leads to a decrease in glacial pCO_2 by 12 ppmv. The sharp decrease of NADW formation at the beginning of the Heinrich event 1 and the YD reduces pCO_2 further by 8 and 6 ppmv, respectively (Figure 8a). This massive and abrupt collapse and rapid resumption of the Atlantic meridional circulation was concluded from $^{231}Pa/^{230}Th$ data [*McManus et al.*, 2004]. These authors also find only a small decline in the Atlantic overturning during the YD cold event. This supports our assumption of only little changes in NADW here and is in contrast to former studies, which attempted to explain the well pronounced peak in atmospheric $\Delta^{14}C$ during the YD with a complete shutdown of deep water formation [e.g., *Stocker and Wright*, 1996; *Delaygue et al.*, 2003]. However, as the $^{231}Pa/^{230}Th$ data carry a mixed information of both export production and ocean circulation only the times of fast changes in the circulation patterns can be identified, while the quantification of changes in the THC is difficult.

[28] Southern Ocean stratification is assumed to collapse at about 17 kyr BP leading to enhanced vertical mixing, in line with oceanic $\delta^{13}C$ data [*Spero and Lea*, 2002; *Hodell et al.*, 2003]. We like to emphasize that the variation of vertical mixing rates as plotted in Figure 6 still allows water mass exchange between Southern Ocean surface and deep waters

during glacial conditions. Prior to 17 kyr BP when the vertical mixing in the Southern Ocean was set to 0 Sv, there still exists an upwelling of 16 Sv (if NADW formation is unchanged) and a downwelling of 9 Sv in the Southern Ocean (Figure 2). Further evidence for a reduced glacial Southern Ocean vertical mixing comes from nutrient records [*François et al.*, 1997; *Crosta and Shemesh*, 2002]. Two modeling approaches [*Gildor et al.*, 2002; *Paillard and Parrenin*, 2004] on long-term variability of atmospheric pCO$_2$ also pinpoint G/IG changes in Southern Ocean vertical mixing as one dominant process important for late Quaternary climate change. While both studies
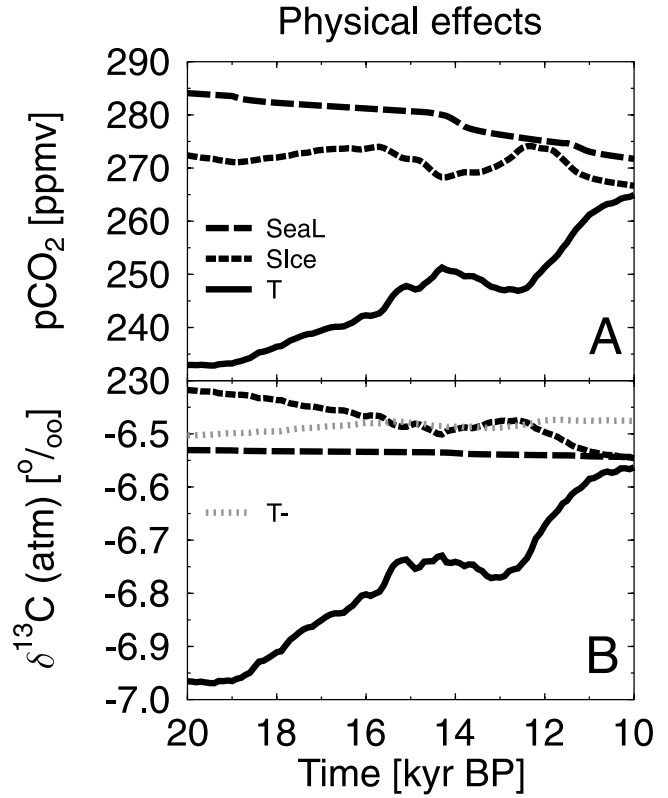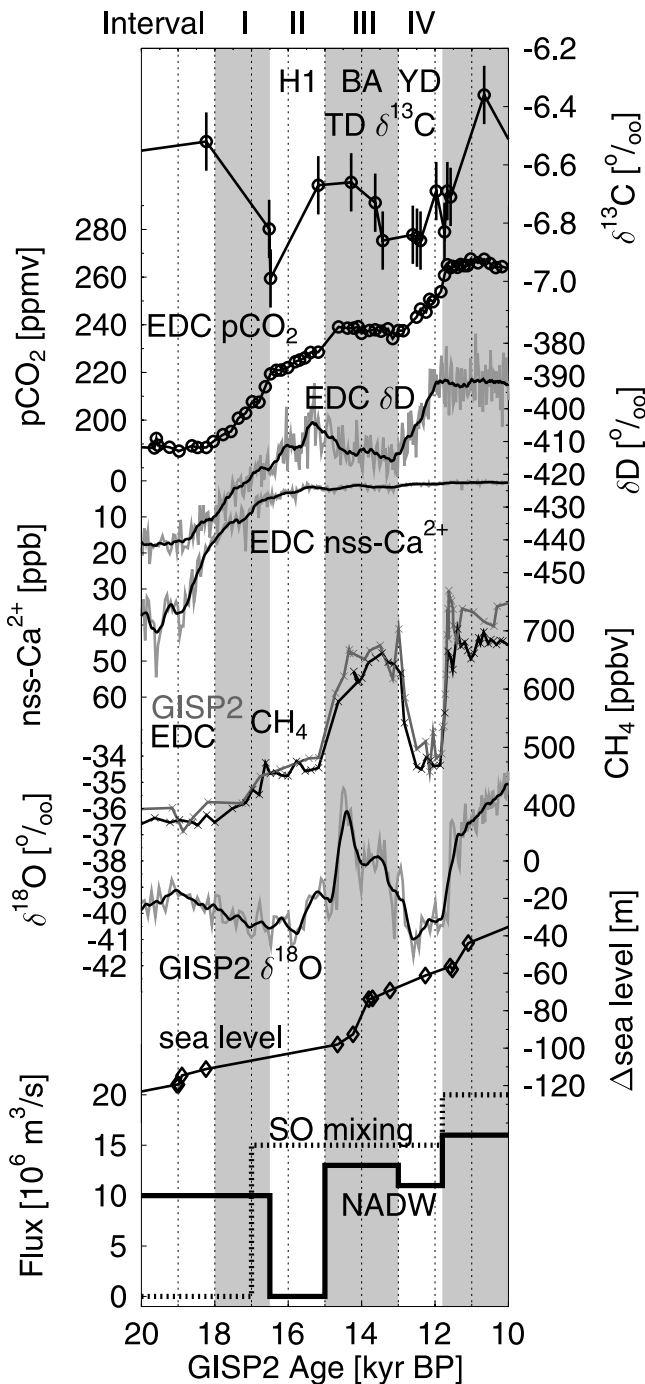
Figure 7. Simulation of physical impacts of sea level rise (SeaL), sea ice extensions (SIce), and temperature effects (T) on atmospheric carbon records, (a) pCO$_2$ and (b) δ^{13}C. The temperature-dependent solubility affects both pCO$_2$ and δ^{13}C, while the temperature-dependent isotopic fractionation during gas exchange only affects δ^{13}C (T-, solubility only, T, combined effects). See color version of this figure in the HTML.

Figure 6. Time-dependent forcing functions of the model during Termination I. Atmospheric δ^{13}C in the Taylor Dome ice core [*Smith et al.*, 1999]; pCO$_2$ in the EPICA Dome C (EDC) ice core divided in four intervals with different changing rates [*Monnin et al.*, 2001]; δD from EDC as isotopic temperature proxies for southern high latitude [*Jouzel et al.*, 2001]; nss-Ca^{2+} record in EDC as proxy for Southern Ocean dust/Fe input [*Röthlisberger et al.*, 2002]; CH$_4$ from EDC and GISP2 ice cores [*Brook et al.*, 1996; *Monnin et al.*, 2001] used for synchronizing EDC records to the GISP2 age scale [*Meese et al.*, 1997]; δ^{18}O from the GISP2 ice core as isotopic temperature proxy for northern high latitude [*Grootes and Stuiver*, 1997]; sea level changes derived from coral reef terraces (on an individual timescale) [*Fairbanks*, 1990]. Strongly fluctuating records (δ^{18}O, δD, nss-Ca^{2+}) are low-pass filtered using a 500-year running mean. The δ^{13}C was synchronized via pCO$_2$ to the atmospheric carbon record of EDC. Shown are also the assumed changes in the amplitude of NADW formation and the strength of vertical mixing in the Southern Ocean over time. See color version of this figure in the HTML.

Ocean circulation
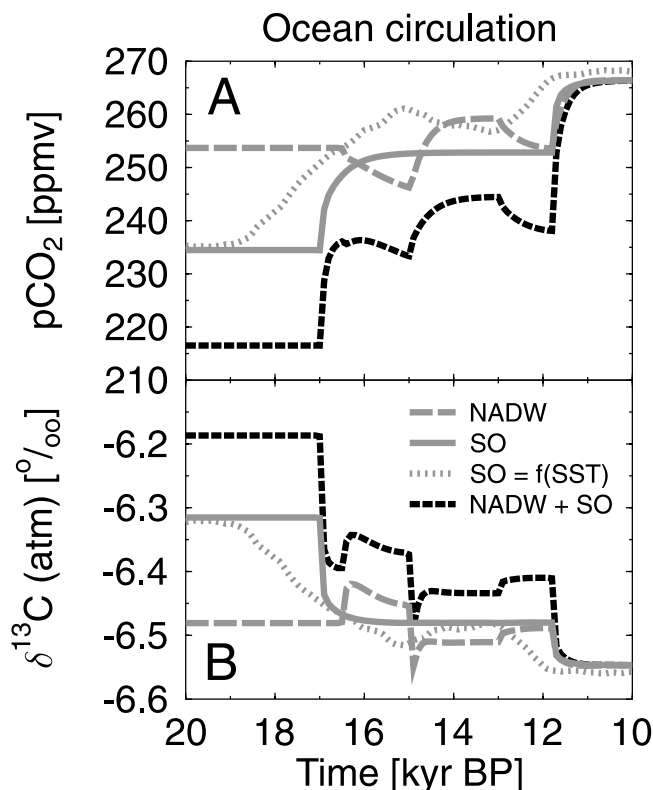
Figure 8. Simulated impacts of time-dependent variations in the strength of NADW formation and Southern Ocean (SO) vertical mixing on atmospheric carbon records, (a) pCO_2 and (b) $\delta^{13}C$. We vary the strength of NADW formation (NADW), or Southern Ocean mixing (SO), or both simultaneously (NADW + SO) as plotted in Figure 6. Alternatively, Southern Ocean mixing is varied as a function of SST (SO = f(SST)). See color version of this figure in the HTML.

propose a physical mechanism for this increase in Southern Ocean water column stratification, they differ in detail. *Gildor et al.* [2002] propose that during glacial times the cooler NADW arriving in the Southern Ocean reduces the rate of vertical mixing there. *Paillard and Parrenin* [2004] explain glacial deep stratification in the Southern Ocean by more saline and thus denser bottom waters which involves brine rejection and is linked to sea ice formation and the Antarctic ice sheet extent.

[29] The breakdown of the Southern Ocean stratification would lead to the release of 37 ppmv of pCO_2 and a drop in $\delta^{13}C$ by 0.25‰ (Figure 8). However, whether the increase in vertical mixing in the Southern Ocean happens rapidly or over several millenia is of importance for the temporal evolution of the signals (see section 6.1). We cannot reproduce the sharp decrease in atmospheric $\delta^{13}C$ around 17 kyr BP if the Southern Ocean vertical mixing rates is, for example, linearly coupled to the temporal evolution of SST (scenario SO = f(SST) in Figure 8).

### 5.3. Biological Pump

[30] The preindustrial biological pump strength of 10 PgC yr^{-1} reduces atmospheric pCO_2 already by more

than 200 ppmv compared to an abiotic ocean [e.g., *Broecker and Peng*, 1986]. As shown in other studies, iron fertilization of glacial marine productivity [*Martin*, 1990] might contribute to 5–45 ppmv of the G/IG change in pCO_2 [*Watson et al.*, 2000; *Ridgwell and Watson*, 2002; *Bopp et al.*, 2003; *Ridgwell*, 2003b]. If G/IG changes in marine export production are assumed to depend on iron (Fe) fertilization, then they are restricted to HNLC regions. The main HNLC areas are the Southern Ocean and the North Pacific, but the latter is only of secondary importance here due to its small extent and the low macro-nutrient concentration in comparison to the Southern Ocean [*Conkright et al.*, 1994; *Röthlisberger et al.*, 2004]. To simulate an aeolian Fe fertilization of the Southern Ocean we take the non-sea-salt-Ca^{2+}-ion concentration (nss-Ca^{2+}) in EDC [*Röthlisberger et al.*, 2002] as proxy for aeolian dust and thus iron input in the Southern Ocean, which might enhance the marine export production if the macro-nutrient concentrations allow an increased productivity. The rise in pCO_2 starts not before 18 kyr BP. We therefore assume an iron unlimited enhanced export productivity in the Southern Ocean prior to 18 kyr BP of 6.4 PgC yr^{-1} (scenario export production variation only), which consumes all available macro-nutrients there. After 18 kyr BP the Southern Ocean marine export production decreases over time toward its preindustrial flux of 3.4 PgC yr^{-1} parallel to the nss-Ca^{2+} decrease.

[31] The proxy nss-Ca^{2+} limits the impact of Fe to times before 16 kyr BP, when nss-Ca^{2+} is higher by 2 orders of magnitude than in the time interval between 16 and 10 kyr BP (Figure 6). If the available macro-nutrients in the Southern Ocean are fully exploited, the glacial export production is 30% (17% in combined scenarios including all processes) larger than its preindustrial value (Figure 9a). This corresponds to a reduction of approximately 20 ppmv in pCO_2 consistent with other modeling studies [*Ridgwell*, 2003b] and a sharp decrease in atmospheric $\delta^{13}C$ by 0.15‰ (Figures 9a and 9b). As marine production always depends on the availability of preformed macro-nutrients, this result is tightly coupled to ocean circulation and the upwelling of re-mineralized nutrients from the deep ocean.

[32] The question whether marine export production in the Southern Ocean was largely increased during glacial times is highly debated based on nitrogen isotopes as proxy of nutrient utilization, comparisons of benthic and planktic $\delta^{13}C$ and other geochemical tracers [e.g., *Duplessy et al.*, 1988; *Charles and Fairbanks*, 1990; *Kumar et al.*, 1995; *François et al.*, 1997; *Anderson et al.*, 1998, 2002; *Frank et al.*, 2000; *Moore et al.*, 2000; *Bopp et al.*, 2003; *Chase et al.*, 2003; *Kohfeld et al.*, 2005]. Interpretations varied largely in the past. For example, an increased glacial export of organic carbon in the Southern Ocean of about 3 PgC yr^{-1} was concluded from an ecosystem based study [*Moore et al.*, 2000] proposing an alternative interpretation of the data presented by *François et al.* [1997], who supported surface water stratification in the Southern Ocean as most important process impacting on the carbon cycle. It is generally agreed that export production south of the Antarctic Polar Front (APF) decreased during glacial times [*François et al.*, 1997; *Anderson et al.*, 1998, 2002; *Frank et al.*, 2000]. The spatial
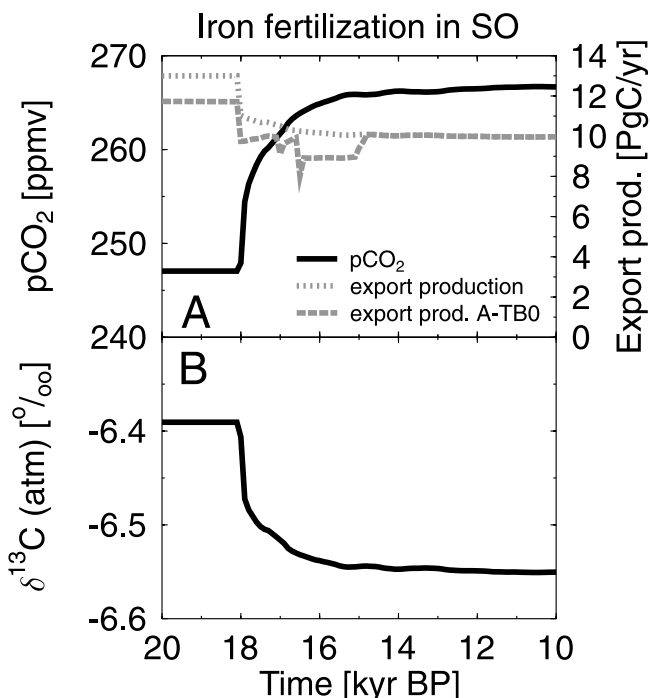
Figure 9. Simulated effects of iron fertilization in the Southern Ocean on atmospheric carbon records, (a) pCO_2 and (b) δ^{13}C. The single process impact of Fe fertilization compared with its impact in the scenario A-TB0 combining all forcings on the marine export production at 100 m water depth is shown additionally. High fluctuations in the export production in A-TB0 are due to macro-nutrient depletion. See color version of this figure in the HTML.

extent of an increased glacial export north of the APF, however, is so far not verified. Data from the Pacific sector of the Southern Ocean [Chase et al., 2003] indicate that the increase in export production found in the Atlantic and Indic sectors [François et al., 1997; Anderson et al., 1998] might not be applicable to other areas. The overall increased export production might be smaller as previously estimated, but was certainly spatially heterogeneous. Data are especially sparse in the largest section of the Pacific sector. It should be noted that our Southern Ocean boxes include the whole ocean area south of 40°S covering also large areas north of the APF. The controversy on glacial Southern Ocean export production is not yet resolved. However, the rise in the integrated glacial export production south of 40°S assumed here appears to be at least consistent with proxy evidence. The determination of its final magnitude still requires further research.

[33] From sediment trap data there is evidence for a coupling of organic and inorganic matter in the sinking particles [Klaas and Archer, 2002; Passow, 2004]. Although the detailed ratio of the exported matter at 100 m water depth cannot be deduced from these studies, they indicate a fairly constant ratio and we therefore do not consider changes in the rain ratio ($r = C_{org}: CaCO_3$) in our standard scenarios, but estimate the impacts of its variation in the following. The range of the rain ratio found in the literature

($r = 4–17$) [e.g., Archer and Maier-Reimer, 1994; Sigman et al., 1998; Sarmiento et al., 2002] would allow an increase of 15 ppmv ($r = 4$), or a decline of less 10 ppmv ($r = 17$) in our preindustrial standard scenario (Figure 3b). One has to keep in mind that in other studies the rain ratio differed between low and high latitudes. Different rain ratios might also be based on different export production fluxes of organic matter. Furthermore, it was hypothesized that a shift in phytoplankton communities from carbonate producing coccolithophores to non-calcifying diatoms might have occurred during glacial times in the Southern Ocean and elsewhere [Brzezinski et al., 2002; Matsumoto et al., 2002]. This would weaken the carbonate pump and change the rain ratio. We estimated the maximum impact of this hypothesis in our modeling context. If we assume that the additional glacial export production of up to 3 PgC yr^{-1} would solely be caused by diatoms, the rain ratio would rise from 10:1 to 13:1, lowering glacial pCO_2 further by less than 8 ppmv. This difference in pCO_2 caused by rain ratio adjustment does not depend on dissolution/sedimentation effects.

[34] It is important to note the water depth at which both export and rain ratio are considered since vertical fluxes of organic matter and $CaCO_3$ are subject to remineralization in the water column. Since some of our surface ocean boxes have a depth of 1000 m, we recalculate fluxes to 100 m water depth, which is most widely used in field surveys.

5.4. Terrestrial Carbon Pools

[35] The terrestrial parts of the BICYCLE model and possible forcing were investigated in detail in a different study [Köhler and Fischer, 2004]. We therefore keep descriptions here very brief. Global area available for land vegetation is calculated from sea level. The residual of competing processes (area loss due to flooding and area gain due to a retreat in land ice sheets) is a vegetation area which is ~5 × 10^{12} m^2 smaller at the LGM than at preindustrial times [Adams and Faure, 1998]. Additionally, the growth of terrestrial biomass is affected by CO_2 and average temperature. To use all boundary conditions available for the G/IG transition, CO_2 fertilization is implemented in a first step in a semi-coupled way, where vegetation growth is calculated as function of prescribed pCO_2 measured in ice cores and not of the internally calculated atmospheric pCO_2. Thus the output of the terrestrial part can be understood as another boundary condition for the ocean/atmosphere module. In the fully coupled mode any offset in the simulations from the pCO_2 data will be amplified owing to the CO_2 fertilization of the biosphere, making a reconstruction of atmospheric carbon over longer times extremely difficult. Global average temperature seen by the terrestrial module is a 3:1 mixture (corresponding to the latitudinal land area distributions in which three fourths of the global land area (excluding Antarctica) is located in the Northern Hemisphere) of GISP2 and EDC temperature proxy with G/IG amplitudes of 8K and 5K in the Northern and Southern Hemisphere, respectively [Kutzbach et al., 1998; Kageyama et al., 2001; Kim et al., 2002]. Thus the terrestrial carbon stocks increase from about 1650 PgC at the LGM to 2200 PgC in the late Holocene, but the parameterization of this transition still
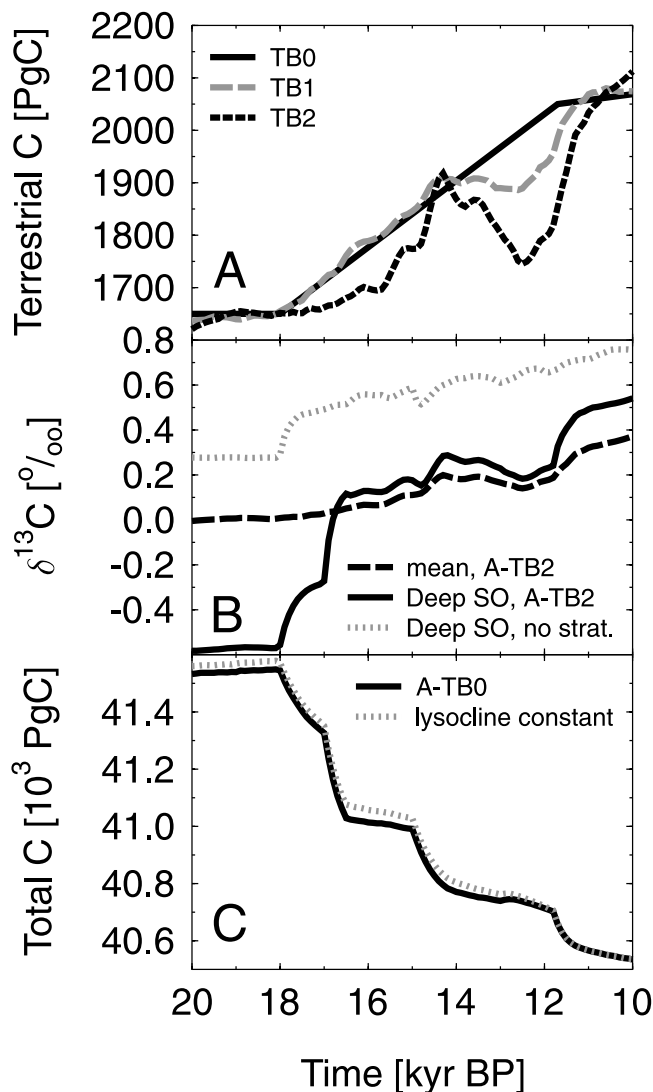
Figure 10. Additional simulation results. (a) Changes in the terrestrial biosphere, scenarios as described in Figure 11. (b) Overall mean change in oceanic $\delta^{13}C$ and in the Southern Ocean $\delta^{13}C$ with (A-TB2) and without changes in Southern Ocean stratification. (c) Total carbon budget of the ocean-atmosphere-biosphere system for scenarios with a constant lysocline or with prescribed changes of the lysocline over time (A-TB0). See color version of this figure in the HTML.

allows various different forcing combinations. Therefore the results of simulations with parameter combinations used by *Köhler and Fischer* [2004] which either follow more a CO_2 fertilization (TB1) or a climate-induced change scenario (TB2) in the terrestrial carbon stock are averaged here. Alternatively (scenario TB0), the terrestrial biosphere grows by 530 PgC from the LGM to preindustrial times with an assumed linear increase of 400 PgC between 18 and 11.8 kyr with a constant fractionation factor of −17‰ (Figure 10a).

[36] For an understanding of the regrowth of the terrestrial biosphere, complex vegetation models are certainly more efficient tools than our model. However, with our simple seven-box module of the terrestrial biosphere we can sketch the main idea of a possible build-up of additional carbon on land. While the total amount of carbon accumulated in the terrestrial pools in the course of the transition is well within the estimates of other studies (see review by *Köhler and Fischer* [2004]), the temporal evolution of the biosphere depends on the physiological response of the biosphere on climate and pCO_2 changes.

[37] In the null-model (scenario TB0), which assumes a linear growth of the terrestrial pools from LGM to the Holocene, atmospheric pCO_2 decreases by 34 ppmv, neglecting $CaCO_3$ compensation (Figure 11a). In the combined scenario using the null-model for the terrestrial pools (A-TB0) the dynamic in $\delta^{13}C$ cannot be explained (Figure 12). This highlights the importance of intrinsic dynamics in the terrestrial part of the carbon cycle. The main difference in the dynamics of TB1 and TB2 is the release of terrestrial carbon during the YD cold event, which leads to a peak of pCO_2 around 13 kyr BP, which is coupled to a drop in $\delta^{13}C$ by 0.3‰ (Figures 10a and 10b).

5.5. Sediment/Ocean Fluxes and Continental Weathering

[38] Besides the amount of carbon transferred from the ocean to the biosphere, the timing and rate of change of the transfer are equally important for the transient response in deep ocean chemistry and atmospheric pCO_2. For example, the transfer of carbon between ocean and biosphere triggers carbonate compensation in the deep sea which in turn affects the time evolution of atmospheric pCO_2. Carbonate compensation is a response to changes in $[CO_3^{2-}]$ in the deep ocean. To counteract these fluctuations in $[CO_3^{2-}]$, the saturation horizon of $CaCO_3$ varies, sedimentation or dissolution rates of $CaCO_3$ change, and deep ocean $[CO_3^{2-}]$ and atmospheric pCO_2 establish a new equilibrium [*Broecker and Peng*, 1987]. We implement sedimentation and dissolution as fluxes of DIC and ALK between the deep ocean and the sediment in our model as follows: We use the current knowledge on shallowing/deepening of the lysocline during Termination I as another boundary condition. The lysocline is the oceanic depth below which sedimentary calcite dissolves. It has been shown that the lysocline during the LGM was about 800 m shallower in the Atlantic and Southern Ocean and 500 m deeper in the Indo-Pacific [*Crowley*, 1983; *Peterson and Prell*, 1985; *Curry and Lohmann*, 1986; *Farrell and Prell*, 1989; *Howard and Prell*, 1994]. We here assume that changes in the lysocline can be approximated by changes in the saturation depth of calcite defined by the intercept of the $[CO_3^{2-}]$ profile in the deep ocean with the saturation concentration of calcite. Both $[CO_3^{2-}]$ and the saturation concentration are a function of temperature, salinity, and pressure. While all state variables such as DIC and ALK and environmental parameters like temperature and salinity are assumed to be homogeneous within one ocean box, pressure and thus $[CO_3^{2-}]$ and the saturation concentration vary with depth and are calculated here in steps of 200 m and interpolated in between. If the modeled saturation depth falls out of the range given by the observations, additional $CaCO_3$ is either dissolved or pre-
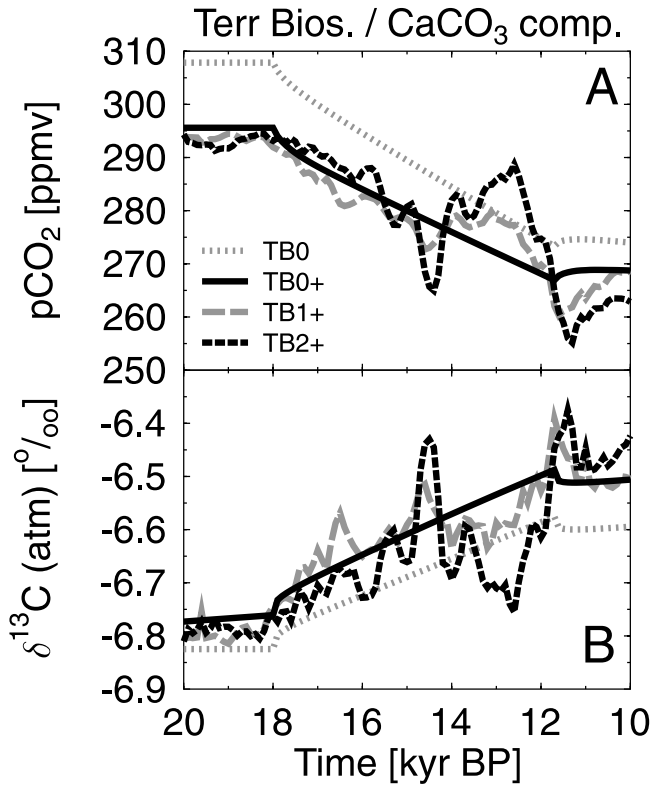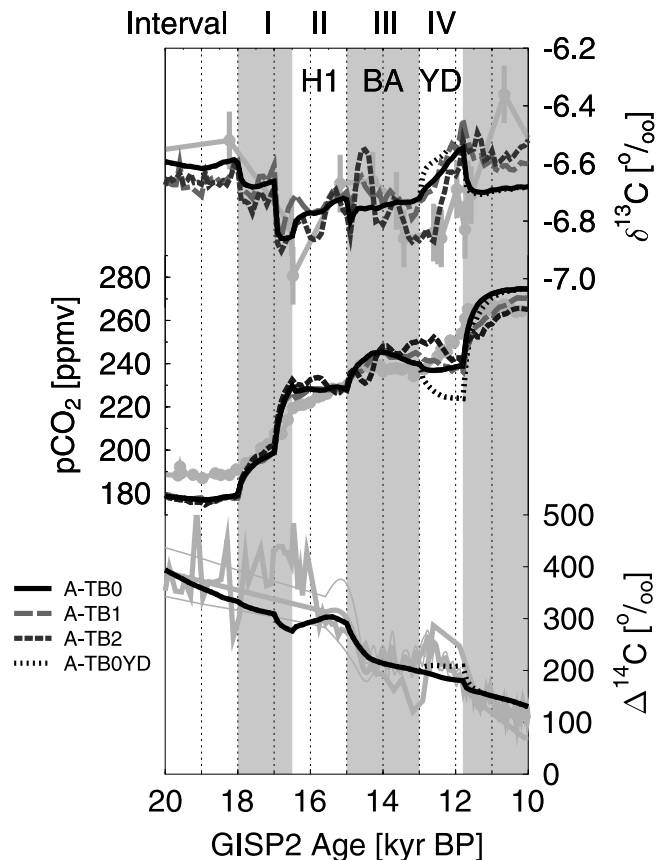
Figure 11. Simulated impacts of changes in the terrestrial biosphere on atmospheric carbon records, (a) pCO_2 and (b) $\delta^{13}C$. Additionally, carbonate compensation is realized by boundary conditions on the G/IG changes in the lyscolines which lead to fluxes of DIC and alkalinity in the ratio 1:2 between sediment and deep ocean. The biosphere follows in a null-model a linear increase (TB0+) or two different dependencies dominated by CO_2 fertilization (TB1+) or climate (TB2+) as plotted in Figure 11a. Sole impact of the growth of the terrestrial biosphere without carbonate compensation is plotted as example for the null model (TB0). See color version of this figure in the HTML.

calculations are now based on an open system where alkalinity and DIC in the atmosphere-ocean-biosphere are not conserved anymore.

[40] If we implement this dissolution/sedimentation mechanism in our model the modeled decrease in pCO_2 caused by the terrestrial regrowth in scenario TB0 is reduced by 7 ppmv due to $CaCO_3$ compensation (Figure 11a). In combined scenarios, including all time-dependent processes, the sedimentation/dissolution mechanism contributes 34 ppmv to the atmospheric rise in pCO_2 during Termination I (Table 2). Even if the lysocline depths are held constant at their preindustrial levels, the changes in the deep ocean carbonate chemistry demand increasing sedimentation over the course of the transition (Figure 10c) which is also in line with a modeling study on atmospheric ^{14}C [Beck et al., 2001]. The mean ocean alkalinity declines by about 5% and the carbon content of the ocean-atmosphere-biosphere is reduced by about 1000 PgC as system response to changes in the global carbon cycle and especially the increased carbon storage on land

cipitated, increasing or decreasing deep ocean $[CO_3^{2-}]$ and thus deepening or shoaling the saturation depth until observations are matched again by the model. Dissolution or precipitation involves the flux of 1 mol DIC and 2 mol ALK between ocean and sediment per 1 mol $CaCO_3$ in the corresponding direction. Vertical gradients in temperature and salinity are very coarse here; a more accurate description which reproduces the observed gradients at a higher resolution might be possible with an advection-diffusion scheme (e.g., Zeebe, submitted manuscript, 2005).

[39] In this first attempt the lysocline in each deep ocean box is assumed to change linearly with time between 18 and 11.8 kyr BP. The implementation of the sedimentation/dissolution mechanism covers the overall inventory changes of ALK in the ocean and carbon in the ocean-atmosphere-biosphere system. Thus it includes implicitly impacts of a reduction in terrestrial weathering inputs of bicarbonate to theses inventories, whose reduced input over the course of the transition would result in an increase in pCO_2 of the order of 9 ppmv [Munhoven, 2002]. Our carbon cycle

Figure 12. Measured and simulated atmospheric carbon records. Data records (gray) are as in Figure 5. Simulation scenarios combine all physical processes (ocean temperature, sea level, sea ice) with changes in ocean circulation (NADW formation, Southern Ocean mixing), marine export production, $CaCO_3$ compensation, and terrestrial biosphere as described in Figure 11. A-TB0YD is same as A-TB0 but with NADW formation shut-off during the Younger Dryas. See color version of this figure in the HTML.

Table 3. Ocean Settings for the 20 kyr BP in Scenario A-TB0[a]

Number	Name	Area, $10^{12} m^2$	Volume, $10^{15} m^3$	Temp, °C	Sal	τ,[b] years	PO_4	O_2	ALK	DIC	$[CO_3^{2-}]$	pCO_2, ppmv	pH	$\delta^{13}C$, ‰	$\Delta^{14}C$, ‰
						Surface Boxes									
1	North Atlantic	16	11	−0.4	35.8	24	0.01	350	2424	2113	216	143	8.40	1.63	265
2	Eq. Atlantic	63	6	17.6	37.3	12	0.04	232	2559	2101	330	197	8.31	1.79	288
3	Southern Ocean	75	73	−0.2	35.6	62	0.35	349	2561	2257	216	166	8.37	1.66	259
4	Eq. Indo-Pacific	176	18	20.1	36.2	15	0.09	223	2600	2109	359	193	8.33	1.56	249
5	North Pacific	14	13	1.4	35	58	2.09	336	2638	2339	217	192	8.33	1.45	222
						Intermediate Boxes									
6	Eq. Atlantic		54	6.8	36.4	86	0.44	249	2553	2207	246		8.31	1.52	263
7	Eq. Indo-Pacific		156	7.5	35.9	86	1.44	107	2598	2333	195		8.17	0.66	205
						Deep Boxes									
8	Atlantic		195	0.0	36.1	359	0.79	232	2204	2095	81		7.87	0.81	204
9	Southern Ocean		209	0.0	35.8	219	2.77	4	2666	2586	79		7.76	−0.50	165
10	Indo-Pacific		562	0.2	35.8	685	3.17	4	2667	2603	71		7.71	−0.44	97
	Whole ocean	344	1298	1.6	35.9	405	2.17	90	2573	2438			7.88	0.08	158
	Atmosphere											179		−6.59	393

[a]Unit of measure is μmol kg^{-1} for PO_4, O_2, ALK, DIC, and $[CO_3^{2-}]$.
[b]Turnover time.

(Figure 10c). The implementation of the compensation mechanism covers also, implicitly, impacts of a reduction in terrestrial weathering inputs to the budgets of alkalinity and DIC, whose variations over the course of the transition would result in an increase in pCO_2 on the order of 9 ppmv [*Munhoven*, 2002]. If, on the other hand, the amount of carbon accumulated in the terrestrial biosphere during the transition is larger than assumed here, the carbonate compensation will counteract this (DGVMs [*Kaplan et al.*, 2002] and other studies based on pollen reconstructions, $\delta^{13}C$ budget analysis, and different modeling approaches (see overview by *Köhler and Fischer* [2004]) tend to propose a G/IG increase of up to 1000 PgC). If we compare a G/IG rise of 500 and 1000 PgC in terrestrial carbon storage in scenarios including $CaCO_3$ compensation, the glacial pCO_2 would be only 10 ppmv higher in the case of the 1000 PgC rise.

[41] It is important to note that the treatment of $CaCO_3$ compensation described above is rather simplistic. It represents a rough estimate of sedimentation/dissolution which is described more accurately (although computationally less efficient) by process-based models of early diagenesis. Owing to ocean circulation, it takes on the order of thousand years until atmospheric pCO_2 reaches a new equilibrium as a response to changes in sedimentation/dissolution reactions. Changes in the depth of the lysocline which are thought to reflect a record of $CaCO_3$ compensation over time are prescribed as boundary conditions. Thus the temporal evolution of $CaCO_3$ compensation with a time-scale of several millennia [*Archer et al.*, 1998] also is not a result of the internal dynamics of our model but prescribed. Fortunately, the temporal evolution of the lysocline is not critical to the model outcome as shown in combined scenarios (Figure 10c).

[42] Neritic carbonate deposition during coral reef build-up in shallow waters is another process of sediment/ocean interaction. Reef growth consumes $CaCO_3$ and is a source for CO_2 in surface waters and was proposed as one possibility to explain the G/IG increase in atmospheric pCO_2 [*Berger*, 1982]. According to a recent data-based study

[*Vecsei and Berger*, 2004] the massive shallow water accumulation of $CaCO_3$ started after melt water pulse (MWP) 1A around 14 kyr BP where sea level rose to about 70 m below present and flooded huge shelf areas and, thus, cannot contribute significantly to the observed pCO_2 rise during the transition. However, most of the coral reef growth of an estimated 370 PgC over the last 14 kyr occurred during the Holocene, peaking around the early Holocene climate optimum (8–6 kyr BP). The reef growth before 10 kyr BP as proposed by *Vecsei and Berger* [2004] was tested with our model, and the influence on pCO_2 is less than 3 ppmv.

6. Temporal Evolution of the Carbon Cycle During Termination I

[43] Combining all relevant processes simultaneously gives us three different realizations depending on the scenario for the regrowth of the terrestrial biosphere. At the LGM all scenarios start with the same carbon cycle conditions of $pCO_2 = 179$ ppmv, $\delta^{13}C = -6.6$‰, and $\Delta^{14}C = 393$‰ (Table 3). Four clearly distinguishable intervals with different rates of change in atmospheric pCO_2 were identified by *Monnin et al.* [2001]. A comparison of simulated and measured atmospheric carbon records over Termination I is compiled in Figure 12.

6.1. Onset of the Rise in pCO_2

[44] Interval I (18.0–16.5 kyr BP on the GISP2 timescale) with pCO_2 increasing at a rate of 20 ppmv kyr^{-1} is accompanied by a drop of 0.5‰ in $\delta^{13}C$ of atmospheric CO_2 and a rather stable $\Delta^{14}C$ during that time. Our simulations reproduce the timing and the smooth increase in pCO_2 at the onset of the transition if we consider Fe fertilization in the Southern Ocean as a process for increased biological productivity and, thus, reduced atmospheric pCO_2 in the LGM. However, since the drop in nss-Ca^{2+}, which we use as a proxy for Fe input into the Southern Ocean, starts already 1 kyr earlier than the pCO_2 increase, Fe seems not to be the limiting factor before 18 kyr BP, and the biological pump in the Southern Ocean implies the existence of a threshold in the aeolian Fe supply

rate as already hypothesized previously for Termination II [*Broecker and Henderson*, 1998]. If $nss-Ca^{2+}$ and, thus, aeolian Fe input are above this threshold prior to 18 kyr BP, the export production in the Southern Ocean is not limited by Fe in the model. Only if both the $nss-Ca^{2+}$ and Fe supply fall below this threshold, i.e., implying a reduction in $nss-Ca^{2+}$ by 1 order of magnitude, Fe becomes the limiting factor of Southern Ocean productivity and progressively more so in the scenario with the further reduction in $nss-Ca^{2+}$ during the following 2 kyr. This threshold below which a reduction in organic export is globally detectable in increasing pCO_2 might be simply a switch from macronutrient limitation (prior to 18 kyr BP) to iron limitation thereafter.

[45] Our simulations reveal that within interval I, only the changes in marine export production together with a breakdown of salinity-driven [*Adkins et al.*, 2002] stratification of the Southern Ocean bringing old, thus, isotopically light carbon to the surface can produce the strong signal in the atmospheric $\delta^{13}C$ (Figures 8a and 8b). Further evidence on the changes in Southern Ocean stratification stems from nutrient records [*François et al.*, 1997] and the G/IG change in $\delta^{13}C$ in benthic foraminifera in the deep Southern Ocean of 1.4‰ [*Hodell et al.*, 2003] which our model only reproduces with the assumed abrupt rise in Southern Ocean ventilation around 17 kyr BP (Figure 10b). We suggest a retreat in winter sea ice in the Southern Ocean as the main cause of the breakdown in Southern Ocean stratification. The reduced melting of salt-depleted sea ice in the sea ice export regions leads to less fresh surface waters in these areas. On the other hand, the production of salty bottom water due to brine rejection during sea ice formation close to the Antarctic continent should be reduced, jointly leading to a destabilization of the water column. Effectively, this process together with any strengthening of wind-drag induced mixing of previously sea ice covered areas acts as an amplifier of any sea ice effect on gas exchange rates [*Stephens and Keeling*, 2000].

6.2. Heinrich Event 1

[46] According to a modeling study [*Knorr and Lohmann*, 2003] the reduction in Southern Ocean winter sea ice acts as a flywheel for the time-delayed resumption of the THC through an increased mass transport of surface waters into the southern Atlantic Ocean. Thus we assume an increased NADW formation at the end of interval II (16.5–15.0 kyr BP, approximately similar to Heinrich event 1) in which the changing rate in pCO_2 slows down to 8 ppmv kyr^{-1}, an increase in $\delta^{13}C$ of 0.4‰ occurs, while the radiocarbon signature decreases sharply at the end of this interval. In detail, NADW formation is shut off during the Heinrich event [*Rahmstorf*, 2002], but resumes to an intermediate strength (13 Sv) thereafter (Figure 6). We are aware that Heinrich event 1 was probably shorter than interval II. According to a recent published review [*Hemming*, 2004], Heinrich event 1 started around 16.8 kyr BP with a duration of 288–1410 years, depending on the observed sediment core. Within the age uncertainty of the ice core records the starting time of interval II (16.5 kyr BP) falls together with the start of Heinrich 1. However, from the data-based

estimate of changes in Atlantic meridional overturning a reduced deep water formation in the North Atlantic very likely exceeds Heinrich 1 until the beginning of the BA warm interval [*McManus et al.*, 2004]. The second main process during interval II which we detect as cause for the increase in the atmospheric carbon isotopic signature is the beginning growth of isotopically light biomass on land (Figures 10a and 11b).

6.3. Bølling-Allerød

[47] Between 15 and 13 kyr BP (BA and interval III) a rather constant atmospheric pCO_2 concentration of 238 ± 1 ppmv is met by a slow decrease in its isotopic signature (−0.2‰), while $\Delta^{14}C$ stays constant in the INTCAL98 record, but decreases with time in the Cariaco basin record. Northern Hemispheric cooling into the YD is expected to result in a reduction in terrestrial carbon stocks and leads to the drop in the isotopic carbon signal (Figures 10a and 11b) in our model in line with the ice core record. The BA warm interval is accompanied by a cooling in the South during the Antarctic Cold Reversal as seen in the EDC δD record (Figure 6) [*Stenni et al.*, 2001] with only little impact on the atmospheric carbon records.

6.4. Younger Dryas

[48] In the final interval (13.0–11.8 kyr BP) of Termination I consisting of the YD, pCO_2 increases again at a rate of 20 ppmv kyr^{-1}. This is accompanied by first constant and then rising $\delta^{13}C$ by 0.4‰. The increase in $\delta^{13}C$ starts in the middle of the YD and is extended 1 kyr into the Holocene. However, the $\delta^{13}C$ signal fluctuates within its uncertainty at the end of the YD which makes the exact termination of its rise difficult. Radiocarbon is rising sharply at the beginning of the YD, then falling again. We propose only a small change in ocean circulation during the YD, supported by our modeled pCO_2 and $\delta^{13}C$ (Figure 12). This implies that observed fluctuations in atmospheric $\Delta^{14}C$ have to be related to changes in the ^{14}C production rate at that time and can not be explained by changes in DWP. The estimate of ^{14}C production rates used here is based on geomagnetic field fluctuations [*Laj et al.*, 2002], used recently by *Hughen et al.* [2004], and agrees for the last 18 kyr with rates calculated from the ^{10}Be record found in ice cores [*Muscheler et al.*, 2004], but uncertainties in both methods of ±10% (relative error) are still large. A shutdown in NADW formation during the YD would explain about half of the observed peak of 100‰ in $\Delta^{14}C$ and result in an increase in $\delta^{13}C$ by 0.2‰ and in a decrease in pCO_2 by 20 ppmv in our model; the latter two are variations which are not found in the ice core records during interval IV (scenario A-TB0YD, Figure 12). Other modeling studies using a zonally averaged global ocean circulation model [*Marchal et al.*, 1998b, 1999, 2001] simulate the YD as a meltwater pulse induced cooling in the North Atlantic. These authors are also not able to explain the observed peak in $\Delta^{14}C$, but their simulated anomaly of rising pCO_2 during the cold event is in line with the ice core data. The dynamics in the simulated pCO_2 in these studies are caused by changes in NADW formation, temperature, and marine export production, as these processes were not uncoupled. Their rise in pCO_2 during the YD was mainly

caused by the reduced marine productivity caused by nutrient depletion in the North Atlantic.

[49] Our modeling results of the $\delta^{13}C$ increase at about 12 kyr BP is composed of two different steps of +0.2‰ within and +0.1‰ shortly after the YD. This differs somewhat from the TD data of first constant $\delta^{13}C$ followed by a rise of 0.4‰ during in the end of the YD. The first step falls together with warming in the Southern Ocean and CO_2 fertilized regrowth of terrestrial carbon stocks during the YD. Temperature dependent fractionation during gas exchange contributes mostly to this signal (Figure 7b). Note that the phasing is highly dependent on the record used for SST in the Southern Ocean. If, for example, the Southern Ocean temperature derived from the EDC deuterium record is replaced by the deuterium excess record from the same ice core [*Stenni et al.*, 2001] representing moisture source temperatures at about 40°S then this difference in modeled versus observed $\delta^{13}C$ would be resolved. The second step is due to the main increase in terrestrial biomass during the Northern Hemispheric warming. A concurrent strengthening of the THC reduces the rise in $\delta^{13}C$ after the YD to about half of its original size (from +0.2 to +0.1‰). An increase in the terrestrial biomass by 250 PgC, about half of the proposed G/IG increase in the terrestrial carbon stocks, over less than 1 kyr is necessary (and according to our model possible, see Figures 10a and 11b) for a rise of more than +0.2‰ in atmospheric $\delta^{13}C$. Accordingly, our model suggests that the terrestrial biosphere depends more on climate (scenario A-TB2) than on CO_2 fertilization effects (A-TB1) on G/IG timescales (Figure 12). However, since our biospheric module does not incorporate spatially resolved aspects the impact of land flooded by sea level rise and the regrowth of boreal forests and tundra in the north after the retreat of the continental ice sheets might be underestimated. Here only the effect that the land area available for vegetation was about 4% smaller at the LGM than at preindustrial times was incorporated [*Köhler and Fischer*, 2004] while the Lund-Potsdam-Jena DGVM calculated that the potential regrowth of the biosphere after the ice retreat was 200 PgG higher than carbon losses on land owing to flooding during the time of the transition [*Joos et al.*, 2004]. Furthermore, these two opposing processes might have been time delayed. Our study nevertheless indicates that fast fluctuations in climate including the YD cold event need to be considered if the G/IG changes in terrestrial carbon are investigated, thus asking for improvements in previous studies [*Kaplan et al.*, 2002; *Joos et al.*, 2004]. In a case study investigating a meltwater flux experiment of 500 years length to the North Atlantic and its subsequent cooling of the Northern Hemisphere the terrestrial carbon pools lose 180 PgC [*Scholze et al.*, 2003]. Results of climate change induced by freshwater discharge experiments on the terrestrial carbon storage in the setting of *Joos et al.* [2004] suggest that the amplitude in carbon storage anomaly might be smaller [*Köhler et al.*, 2005].

7. Discussion

7.1. When Time Matters

[50] This study is an improvement over many steady state simulations done in the past. So far, it was concluded from an inverse modeling study analyzing steady state simulations of a carbon cycle box model with seven oceanic boxes that uncertainties in proxy data and models are still too large to confidently choose one scenario responsible for observed variations in pCO_2 [*LeGrand and Alverson*, 2001]. By introducing the time domain as a fourth target dimension beside pCO_2, $\delta^{13}C$, and $\Delta^{14}C$ our transient modeling approach (in contrast to steady state simulations) is capable of disentangling the effects of various processes operating on the global carbon cycle on G/IG timescales. However, as soon as the time domain becomes important, the robustness of our interpretation also depends on the quality of the synchronization of various records on the same age scale. In the following we therefore discuss some aspects of age uncertainty imprinted in the paleo records and of the timing of certain processes.

[51] The Taylor Dome $\delta^{13}C$ is arguably the least reliable data set used here in terms of age constraint and uncertainty. Therefore our interpretation has to be understood as a rough estimate of the impacts of various processes on the carbon cycle. Especially the timing of the oceanic reorganization which we deduce from modeling based assumptions and the reproduction of our target records might be taken with caution. For example, the timing of the stratification breakdown in the Southern Ocean might vary by about ±500 years. From the sequence of events explaining the resumption of ocean circulation during the transition [*Knorr and Lohmann*, 2003] a delay of about 2 kyr of the abrupt strengthening of the THC around 15 kyr BP after the Southern Ocean sea ice retreat was proposed. As this sea ice retreat is directly connected with the stratification breakdown, it seems not likely that the onset of the pCO_2 increase 3 kyr prior to the THC resumption at approximately 18 kyr BP was initialized by Southern Ocean vertical mixing, but it cannot be excluded owing to the uncertainties of the age scales of the ice cores and our model. Eventually, new $\delta^{13}C$ records with high temporal resolution to be derived from the new EPICA ice cores [e.g., *Leuenberger et al.*, 2003] will resolve finer structures and may lead to an improved interpretation of changes in the carbon cycle over G/IG timescales. However, first results from the EPICA ice cores show high data scatter likely related to the enclosure process of the air bubbles which make it difficult to reproduce known patterns of other ice cores, leaving the question of data uncertainty still open [*Eyer*, 2004].

[52] Furthermore, the two following simplifications might be crucial for the modeling results: First, the length of the reduction in NADW formation during Heinrich event 1 and YD might be too long. It is known that the climate system might need more than 500 years to regain initial temperatures after the end of a freshwater pulse mimicking the processes of a Heinrich event [e.g., *Marchal et al.*, 1998a, 1998b; *Clark et al.*, 2002; *Knutti et al.*, 2004]. Thus the NADW formation might resume earlier at the end of the cold events than the temperature maxima in the north. Second, the low-pass filtering of the ice core temperature proxies especially in the north reduces the abruptness of the Northern Hemisphere temperature fluctuations, for example, stretching the warming at the end of the YD from less than a century to nearly half a millennium. The simulated

response of both pCO_2 outgassing through ocean warming and changes in terrestrial carbon storage are therefore delayed. Both these processes would inflict on the carbon cycle by an earlier rise in pCO_2 and would therefore reduce the still existing offsets between simulation results and data sets (Figure 12).

7.2. The Weak Link: Enhancing the Biological Pump

[53] As reviewed in section 5.3, there is evidence for enhanced glacial export production in the Southern Ocean (south of 40°S) through iron fertilization, although it is still a matter of debate. This enhancement of the biological pump was assumed here as this process would, beside its downdraw of pCO_2, reduce atmospheric $\delta^{13}C$ precisely at the right time during the onset of the rise in pCO_2 at 18 kyr BP. Given the uncertainties in the Taylor Dome $\delta^{13}C$ records discussed earlier, the question arises which alternative scenarios are possible and whether there is other evidence for an enhanced glacial export. Some recent studies set upper limits to the impact of an enhancement of Southern Ocean export production through Fe fertilization. *Röthlisberger et al.* [2004] conclude an upper limit of 20 ppmv from an Antarctic ice core perspective. They compare reductions in the aeolian dust content during Termination I and the Antarctic warming events between 60 and 30 kyr BP, which parallel atmospheric pCO_2 peaks of up to 20 ppmv. However, biological or physical processes of iron utilization and uptake are not considered any further. The modeling study of *Bopp et al.* [2003] sets an upper limit of the pCO_2 increase mediated through iron to 30 ppmv, but a variety of model-based scenarios span the range of 5–45 ppmv (see review by *Ridgwell* [2003b]). In a recent review on the role of marine biology on G/IG pCO_2 it was stated that iron fertilization and associated mechanisms can be responsible for no more than half of the observed variations [*Kohfeld et al.*, 2005]. The reassessment of N-isotopes [*Robinson et al.*, 2004] restricts the enhancement of Southern Ocean productivity further, and the question arises whether there are alternative scenarios to be considered.

[54] One attractive alternative scenario is the silicic acid leakage hypothesis [*Brzezinski et al.*, 2002; *Matsumoto et al.*, 2002] which is also based on Fe fertilization as initial trigger and would thus have a similar temporal evolution as our initial Fe fertilization approach. Briefly, this hypothesis assumes that the Fe fertilization in the Southern Ocean initiates a reduced Si:N uptake ratio in diatoms there. This leads to a northward propagation of un-utilized silicic acid. In middle to low latitudes, modifications in nutrient concentrations shift phytoplankton community assemblages toward diatoms, which then can increase their export production there. The down-draw of pCO_2 through higher organic matter fluxes would be accompanied by local changes in the rain ratio (a weaker carbonate pump) which would additionally reduce pCO_2. Unfortunately, in our present model setup we are unable to test this scenario, as glacial macro-nutrient concentrations in the equatorial surface ocean boxes do not allow any further enhancement in marine export production. We have to acknowledge that our preindustrial biological productivity in low latitudes is already 30% smaller than deduced from data-based inverse

modeling studies [*Schlitzer*, 2000]. Therefore our modeling restriction cannot falsify the silicic acid leakage hypothesis.

[55] As a further alternative, the enhancement of marine glacial export production in the North Pacific, another HNLC region, might be a process of interest. The upper limit of its impact was estimated to 9 ppmv [*Röthlisberger et al.*, 2004].

[56] In summary, we believe that the marine biology plays a role in the quest of explaining the observed G/IG rise in pCO_2. Its magnitude seems to be on the order of 20 ppmv, but details need to be clarified by further studies.

7.3. Evidence From Paleoceanographic $\delta^{13}C$ Data

[57] What data evidence is there for the reliability of our ocean setting during the LGM as summarized in Table 3? To challenge our results with paleo data we compare the evolution of oceanic $\delta^{13}C$ across Termination I in our model with $\delta^{13}C$ of benthic foraminifera (Figure 13).

[58] Depending on the selection of sediment cores, the $\delta^{13}C$ signal recorded in benthic foraminifera increased from LGM to preindustrial times by 0.30–0.46‰ [*Curry et al.*, 1988; *Duplessy et al.*, 1988]. The rise is largest (0.8‰) in the deep Southern Ocean [*Curry et al.*, 1988; *Curry and Oppo*, 2005] with maximum differences (1.4‰) in waters below 2500 m [*Hodell et al.*, 2003]. The Indo-Pacific and the Atlantic Ocean exhibit significant smaller amplitudes of 0.4–0.5‰ [*Curry et al.*, 1988; *Boyle*, 1992], while the $\delta^{13}C$ rise also varies with depth. Particularly, in the Atlantic, $\delta^{13}C$ shifts from a G/IG drop in waters above 2000 m to a rise in waters below [*Boyle*, 1992; *Oppo and Lehman*, 1993; *Curry and Oppo*, 2005].

[59] We simulate a mean rise in oceanic $\delta^{13}C$ of 0.36‰ from LGM to preindustrial times (Tables 1 and 3). Further, our simulations reveal a G/IG rise in $\delta^{13}C$ in the deep Atlantic, Southern Ocean, and Indo-Pacific of −0.15‰, 1.07‰, and 0.54‰, respectively (Tables 1 and 3). While the rise in the Southern Ocean and Indo-Pacific are at the upper range of reconstructions, the drop in the Atlantic Ocean is only found in the upper 2 km of the water column. This could indicate that either ocean circulation pattern in the Atlantic changed differently than assumed here or that marine export production was increased during glacial times in equatorial regions as suggested by the "silicic acid leakage hypothesis" [*Brzezinski et al.*, 2002; *Matsumoto et al.*, 2002].

[60] Nevertheless, across Termination I, our simulation of deep ocean $\delta^{13}C$ covers the temporal evolution of selected records of $\delta^{13}C$ in benthic foraminifera rather well (Figure 13). The amplitude is slightly larger in the simulation than in the Indo-Pacific data, and offset by 0.5‰ to more positive values in the Southern Ocean. In the Atlantic the simulated amplitude is slightly smaller than in the data, but our simulation seems to cover millennial-scale variations on the order of 0.5‰ across the transition. Furthermore, our simulations show a distinct negative peak in $\delta^{13}C$ of 1–2‰ in equatorial surface and intermediate waters, parallel with a peak of 0.3‰ in the North Atlantic, probably caused by the shutdown of the NADW formation during Heinrich event 1. The simulation predict a decline in $\delta^{13}C$ of 0.2‰ in the
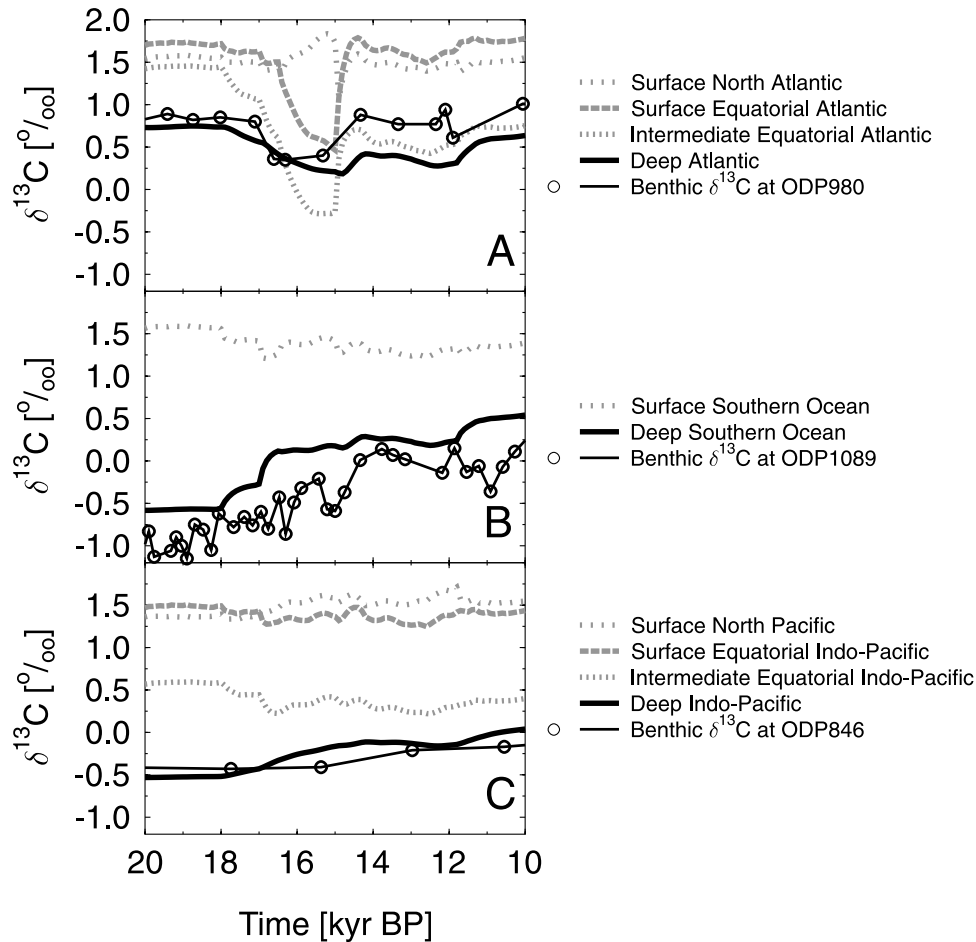
Figure 13. Temporal evolution of oceanic $\delta^{13}C$ in all ocean boxes over Termination I in comparison to selected data records of $\delta^{13}C$ in benthic foraminifera. (a) Atlantic Ocean. Data are from *C. wuellerstorfi* in core ODP980 (55°29′N, 14°42′W, 2179 m water depth) [*McManus et al.*, 1999]. (b) Southern Ocean. Data are from *Cibicidoides* spp. in core ODP1089 (40°56′S, 9°54′E, 4621 m water depth) [*Hodell et al.*, 2002; *Hodell et al.*, 2003]. (c) Indo-Pacific Ocean. Data are from *C. wuellerstorfi* and *U. peregrina* in core ODP846 (3°5′S, 90°82′W, 3296 m water depth) [*Mix et al.*, 1995]. See color version of this figure in the HTML.

Southern Ocean and rather stable $\delta^{13}C$ values in the surface waters of the Indo-Pacific (a slight increase of +0.2‰ in the equatorial regions, and a slight decrease of −0.1‰ in the north).

[61] The simulated negative excursion in intermediate Atlantic waters is significant and should therefore be traceable in sediment records. There is some evidence for a decline of 0.5−1.0‰ in $\delta^{13}C$ from a selection of cores of intermediate depth (400−1500 m) from the Bahamas [*Slowey and Curry*, 1995]. However, as age models in this study were developed only for two out of nine cores, it is difficult to interpret if the minima in $\delta^{13}C$ seen in these cores occurred during the transition or later on in the early Holocene. We refrain from a comparison of modeled surface water $\delta^{13}C$ with data derived from planktic foraminifera, as planktic $\delta^{13}C$ can be heavily overprinted by various effects (disequilibrium, dissolution, habitat, carbonate ion effect) [*Spero et al.*, 1997; *Mulitza et al.*, 1999]. Therefore the interpretation of surface $\delta^{13}C$ data is limited and might need further work in order to understand under-

lying processes affecting stable carbon isotope fractionation in planktic foraminifera.

[62] We emphasize that the $\delta^{13}C$ model-data comparison gives some insights into model performance but provides only a restricted evaluation of the entire model outcome. Compilations of freely available data sets were chosen here as representative for certain ocean basins. However, this particular choice does not necessarily represent the actual average basin-$\delta^{13}C$ values across the transition, and therefore the optimal validation target for the average $\delta^{13}C$ values of our ocean model boxes.

7.4. Robustness of Our Results

[63] In the light of the uncertainties of our approach discussed above, the question arises how robust our final G/IG scenarios are. While the timing and magnitude of several processes are well documented, others still allow a range of possible implementations. Below we discuss the robustness of all major processes summarized in Table 2. In doing so, we focus on their reliability and give an estimate

on their credibility in our present carbon cycle model and in comparison with other modeling results.

7.4.1. Sea Level Rise (Highly Credible)

[64] In the context of our study the resolution of sea level reconstruction and its timing based on coral records [*Fairbanks*, 1990] is sufficient. Other studies report results of the same order of magnitude as ours, for example, a reduction of pCO_2 during Termination I by 7 ppmv [*Matsumoto et al.*, 2002].

7.4.2. Ocean Temperatures (Credible) and Sea Ice (Fairly Credible, But Model Dependent)

[65] Multiproxy approaches seemed to be the best estimates to derive reliable temperature proxies. There might be improvements through new sediment cores and better methodologies, but in the coarse resolution of our model this might alter our pCO_2 estimates only very little. The time-slice reconstruction of sea ice coverage is still improving for the LGM [e.g., *Gersonde et al.*, 2005]. Again, the limitations of our model design restrict any fundamental changes through an updated sea ice coverage. However, it has to be kept in mind (as discussed earlier) that the impact of sea ice and thus gas-exchange on pCO_2 is strongly model dependent [*Archer et al.*, 2003].

7.4.3. Ocean Circulation (Fairly Credible)

[66] Our knowledge on changes in NADW formation were improved greatly in the past years. Especially the possibility to fix the resumptions of the NADW in time is of importance in this context. The magnitude of the NADW formation might in detail still be a matter of debate (e.g., in the Younger Dryas), but the general picture that emerges so far seems to be stable. The circulation in the Indo-Pacific was kept constant in our scenarios, which is supported by $\delta^{13}C$ [*Mix et al.*, 1991] and $\Delta^{14}C$ [*Broecker et al.*, 2004] data, suggesting that the glacial ventilation of the deep Pacific Ocean was not much different from today's situation. However, it has to be stressed that the understanding of ocean circulation strength is still limited. Circulation patterns calculated from full OGCMs for the present-day situation vary still considerably from each other and from observations, as shown in the Ocean Carbon-cycle model Inter-comparison Project (OCMIP) [e.g., *Doney et al.*, 2004].

7.4.4. Shallow Water Carbonate Production (Fairly Credible)

[67] The data constraints limit the impact of coral reef growth on pCO_2 during Termination I [*Vecsei and Berger*, 2004] especially via the time domain as their contribution is tightly coupled to sea level rise above 70 m below present. We therefore argue that the coral reef hypothesis as the dominant process explaining the G/IG rise in pCO_2 is rather unlikely. However, the magnitude of the pCO_2 rise caused by shallow water contributions (so far $1-3$ ppmv) might increase slightly through carbonate accumulation besides that of coral reefs, for example, through accumulation on isolated banks [*Vecsei*, 2004].

7.4.5. Terrestrial Biosphere (Fairly Credible)

[68] Data and models nowadays agree that the carbon storage on land increased during Termination I; its magnitude, however, is still a matter of debate. We estimate that the overall rise in terrestrial carbon as well as the large perturbation during the YD cold interval imprint an uncertainty of about 10 ppmv onto our results. This is based on intercomparsions of DGVMs [*Cramer et al.*, 2001] and the sensitivity of individual models to different climate forcings, as seen from studies mimicking a NADW shutdown and its consequent cooling of the Northern Hemisphere [*Scholze et al.*, 2003; *Köhler et al.*, 2005].

7.4.6. Southern Ocean Vertical Mixing (Fairly Credible)

[69] There is evidence for decreased glacial Southern Ocean water column stratification from various records, different proxies and the support by modeling studies [e.g., *François et al.*, 1997; *Crosta and Shemesh*, 2002; *Hodell et al.*, 2003; *Gildor et al.*, 2002; *Paillard and Parrenin*, 2004]. However, here our results demand an abrupt increase in vertical mixing rates at the onset of the pCO_2 rise to reconstruct especially the evolution of the atmospheric $\delta^{13}C$ record. Robust evidence from proxy reconstructions on the timing and the velocity of the changes are hard to find. Therefore our assumption of the rapid increase in mixing can be understood as a result of our study, which asks for verification from more complex physical ocean models or new paleoceanographic data sets. As this process explains the largest part of the G/IG rise in pCO_2 and most of the 0.5‰ drop in $\delta^{13}C$ at 17 kyr BP, large changes here would significantly impact our modeling results. Again, it has to be said that different models might come up with different results [*Archer et al.*, 2003]. Therefore the question is not only what support our approach has from paleo data sets, but also what the model-dependent answer to it might be.

7.4.7. Sediment/Ocean Exchange Fluxes (Fairly Credible)

[70] The global pattern of changes in the lysocline are fairly well known. However, all paleo-reconstructions of carbonate production so far are based on the large shell-size fraction ($>63~\mu m$) neglecting any impact of smaller individuals. The calculation of the carbonate saturation depth with our box model is also a rough estimate, as temperature and salinity (which together with pressure determine the saturation depth) do vary with depth in nature, but were kept constant below 1000 m in our model. Minor improvements can be expected if not only net changes in the DIC and ALK inventories were modeled, but the riverine input of weathering products would be accounted for separately. These improvements would only modify details of the overall behavior of the carbonate cycle. Further improvement can also be expected from process-based modeling of sediment diagenesis. We nevertheless believe that the global scale impacts of sedimentation/dissolution are captured fairly well in our approach.

7.4.8. Biological Pump (Uncertain)

[71] As outlined in the previous section, the detailed response of the marine biology is not well constrained. Data point to a constant rain ratio which tightly connects the soft tissue and the carbonate pump. Iron fertilization seems to be a tempting hypothesis explaining up to 20 ppmv of the pCO_2 rise. However, so far one can only speculate about the details of shifts in community structure or enhanced glacial export production. It would be, on the other hand, very

surprising if major physical and biogeochemical parameters changed, but the export production of the marine biology stayed constant over time.

7.4.9. Summary

[72] In summary, our approach was based on the implementation of highly credible processes first. The more uncertain processes were added later on. We like to emphasize that we did not fine-tune uncertain processes such as the impact of the biological pump to accurately match the ice core observations. We are aware of its limited reliability and therefore ask for other studies detailing single parts of the carbon cycle to disentangle still open questions.

8. Conclusions

[73] The processes causing relevant changes on pCO_2 as summarized in Table 2 are all important during the last termination and in line with the temporal development of the atmospheric carbon records (Figure 12). They are, in decreasing order of their impact on pCO_2: the rise in Southern Ocean vertical mixing rates (>30 ppmv), decreases in alkalinity and carbon inventories (>30 ppmv), the reduction of the biological pump (~20 ppmv), the rise in ocean temperatures (15–20 ppmv), the resumption of ocean circulation (15–20 ppmv), and coral reef growth (<5 ppmv). The regrowth of the terrestrial biosphere, sea level rise and the increase in gas exchange through reduced sea ice cover operate in the opposite direction, decreasing pCO_2 during Termination I by ~30 ppmv. While the dynamic of the physical system seems to be constrained rather well by proxy data, changes in biogeochemical processes are more uncertain. All the major processes contributing to the G/IG pCO_2 change seem to be identified, although the size of their contributions may have to be revised. Nevertheless, disentangling different processes over the course of the transition as done here is the only way to gain insights into causes of temporal changes in the data records. For example, a study based on steady state simulations for the LGM and preindustrial times undertaken with an Earth system model of intermediate complexity concludes that the initial drop in $\delta^{13}C$ might have been caused by an enhanced marine biological pump during the LGM [*Brovkin et al.*, 2002]. We argue that a complete picture of G/IG change only emerges if all subsequent temporal variations in both atmospheric carbon records can be addressed. Therefore the conclusions of *Brovkin et al.* [2002] may have to be revised based on the importance of Southern Ocean stratification breakdown at the onset of the termination as proposed here.

[74] According to our model assumptions, which are bound as closely as possible to data constraints, we are able to reproduce the temporal evolution of the atmospheric carbon records during Termination I. While this approach does not exclude other scenarios, we emphasize that alternatives scenarios also need to be able to reproduce the time-dependent development of as many variables of the carbon cycle as possible. A plausible scenario of the sequence of events during the last deglaciation according to this study is the following. (1) starting in 18 kyr BP, a reduction in aeolian Fe input into the Southern Ocean results in lower marine export production to the deep ocean and an outgas-

sing of CO_2. (2) Parallel to Southern Hemisphere warming, Southern Ocean winter sea ice cover is largely reduced and leads to the breakdown of Southern Ocean stratification (~17 kyr BP). (3) The reduced Southern Ocean sea ice opens water transport ways into the Atlantic Ocean and acts, after the shutdown of NADW formation during Heinrich event 1 (16.5–15 kyr BP), as a flywheel on the THC. With a delay of about 1.5–2 kyr, NADW formation resumes with at least intermediate strength. (4) In addition to a further strengthening of the THC after the YD, during which the strength of the NADW formation is only slightly reduced, the most relevant changes to pCO_2 and $\delta^{13}C$ during the BA and the YD (15–11.8 kyr BP) are CO_2 fertilization and Northern Hemispherical temperature changes modifying the carbon storage in the terrestrial biosphere. (5) Coral reef growth with a subsequent outgassing of CO_2 starts only after MWP 1A (14 kyr BP) and initially only at a marginal rate.

References

Adams, J. M., and H. Faure (1998), A new estimate of changing carbon storage on land since the Last Glacial Maximum, based on global land ecosystem reconstruction, *Global Planet. Change*, *16–17*, 3–24.

Adkins, J. F., K. McIntyre, and D. P. Schrag (2002), The salinity, temperature, and $\delta^{18}O$ of the glacial deep ocean, *Science*, *298*, 1769–1773.

Aeschbach-Hertig, W., F. Peeters, U. Beyerle, and R. Kipfer (2000), Palaeotemperature reconstruction from noble gases in ground water taking into account equilibration with entrapped air, *Nature*, *405*, 1040–1044.

Alley, R. B., and P. U. Clark (1999), The deglaciation of the Northern Hemisphere: A global perspective, *Annu. Rev. Earth Planet. Sci.*, *27*, 149–182.

Amiotte-Suchet, P., J.-L. Probst, and W. Ludwig (2003), Worldwide distribution of continental rock lithology: Implications for the atmospheric/soil CO_2 uptake by continental weathering and alkalinity river transport to the oceans, *Global Biogeochem. Cycles*, *17*(2), 1038, doi:10.1029/2002GB001891.

Anderson, R. F., N. Kumar, R. A. Mortlock, P. N. Froelich, P. Kubik, B. Dittrich-Hannen, and M. Suter (1998), Late-Quaternary changes in productivity of the Southern Ocean, *J. Mar. Syst.*, *17*, 497–514.

Anderson, R. F., Z. Chase, M. Q. Fleisher, and J. Sachs (2002), The southern Oceans's biological pump during the Last Glacial Maximum, *Deep Sea Res., Part II*, *49*, 1909–1938.

Archer, D. (1991), Modelling the calcite lysocline, *J. Geophys. Res.*, *96*(C9), 17,037–17,050.

Archer, D., and E. Maier-Reimer (1994), Effect of deep-sea sedimentary calcite preservation on atmospheric CO_2 concentration, *Nature*, *367*, 260–263.

Archer, D., H. Kheshgi, and E. Maier-Reimer (1998), Dynamics of fossil fuel neutralization by marine $CaCO_3$, *Global Biogeochem. Cycles*, *12*(2), 259–276.

Archer, D., A. Winguth, D. Lea, and N. Mahowald (2000a), What caused the glacial/interglacial atmospheric pCO_2 cycles?, *Rev. Geophys.*, *38*(2), 159–189.

Archer, D. E., G. Eshel, A. Winguth, W. Broecker, R. Pierrehumbert, M. Tobis, and R. Jacob (2000b), Atmospheric pCO_2 sensitivity to the biological pump in the ocean, *Global Biogeochem. Cycles*, *14*(4), 1219–1230.

Archer, D. E., P. A. Martin, J. Milovich, V. Brovkin, G.-K. Plattner, and C. Ashendel (2003), Model sensitivity in the effect of Antarctic sea ice and stratification on atmospheric pCO_2, *Paleoceanography*, *18*(1), 1012, doi:10.1029/2002PA000760.

Barnola, J. M., D. Raynaud, Y. S. Korotkevich, and C. Lorius (1987), Vostok ice core provides 160,000-year record of atmospheric CO_2, *Nature*, *329*, 408–414.

Beck, J. W., D. A. Richards, R. L. Edwards, B. W. Silverman, P. L. Smart, D. J. Donahue, S. Hererra-Osterheld, G. S. Burr, L. Calsoyas, A. J. T. Jull, and D. Biddulph (2001), Extremely large variations of atmospheric ^{14}C concentration during the last glacial period, *Science*, *292*, 2453–2458.

Becquey, S., and R. Gersonde (2003), A 0.55-Ma paleotemperature record from the subantarctic zone: Implications for the Antarctic Circumpolar Current development, *Paleoceanography*, *18*(1), 1014, doi:10.1029/2000PA000576.

Berger, W. H. (1968), Planktonic foraminifera: Selective solution and paleoclimatic interpretation, *Deep Sea Res.*, *15*, 31–43.

Berger, W. H. (1982), Increase of carbon dioxide in the atmosphere during deglaciation: The coral reef hypothesis, *Naturwissenschaften*, *69*, 87–88.

Berger, W. H., and R. S. Keir (1984), Glacial-Holocene changes in atmospheric CO_2 and the deep-sea record, in *Climate Processes and Climate Sensitivity*, *Geophys. Monogr. Ser.*, vol. 29, edited by J. E. Hansen and T. Takahashi, pp. 337–351, AGU, Washington, D. C.

Bopp, L., K. E. Kohfeld, and C. L. Quere (2003), Dust impact on marine biota and atmospheric CO_2 during glacial periods, *Paleoceanography*, *18*(2), 1046, doi:10.1029/2002PA000810.

Boyle, E. A. (1992), Cadmium and $\delta^{13}C$ paleochemical ocean distributions during the stage 2 glacial maximum, *Annu. Rev. Earth Planet. Sci.*, *20*, 245–287.

Broecker, W. S., and G. M. Henderson (1998), The sequence of events surrounding Termination II and their implications for the cause of glacial-interglacial CO_2 changes, *Paleoceanography*, *13*(4), 352–364.

Broecker, W. S., and T. H. Peng (1986), Carbon Cycle 1985: Glacial to interglacial changes in the operation of the global carbon cycle, *Radiocarbon*, *28*, 309–327.

Broecker, W. S., and T.-H. Peng (1987), The role of $CaCO_3$ compensation in the glacial to interglacial atmospheric CO_2 change, *Global Biogeochem. Cycles*, *1*(1), 15–19.

Broecker, W. S., and T. Takahashi (1978), The relationship between lysocline depth and in situ carbonate ion concentration, *Deep Sea Res.*, *25*, 65–95.

Broecker, W., J. Lynch-Stieglitz, D. Archer, M. Hofmann, E. Maier-Reimer, O. Marchal, T. Stocker, and N. Gruber (1999), How strong is the Harvardton-Bear constraint?, *Global Biogeochem. Cycles*, *13*(4), 817–820.

Broecker, W., S. Barker, E. Clark, I. Hajdas, G. Bonani, and L. Stott (2004), Ventilation of the glacial deep Pacific Ocean, *Science*, *306*, 1169–1172.

Brook, E. J., T. Sowers, and J. Orchardo (1996), Rapid variations in atmospheric methane concentration during the past 110,000 years, *Science*, *273*, 1087–1091.

Brovkin, V., M. Hofmann, J. Bendtsen, and A. Ganopolski (2002), Ocean biology could control atmospheric $\delta^{13}C$ during glacial-interglacial cycle, *Geochem. Geophys. Geosyst.*, *3*(5), 1027, doi:10.1029/2001GC000270.

Brzezinski, M. A., C. J. Pride, V. M. Franck, D. M. Sigman, J. L. Sarmiento, S. K. Matsumoto, N. Gruber, G. H. Rau, and K. H. Coale (2002), A switch from $Si(OH)_4$ to NO_3- depletion in the glacial Southern Ocean, *Geophys. Res. Lett.*, *29*(12), 1564, doi:10.1029/2001GL014349.

Cavalieri, D. J., P. Gloersen, C. L. Parkinson, J. C. Comiso, and H. J. Zwally (1997), Observed hemispheric asymmetry in global sea ice changes, *Science*, *278*, 1104–1106.

Charles, C. D., and R. G. Fairbanks (1990), Glacial to interglacial changes in the isotopic gradients of Southern Ocean surface water, in *Geological History of the Polar Oceans: Artic Versus Antarctic*, edited by U. Bleil and J. Thiede, pp. 519–538, Springer, New York.

Charles, C. D., and R. G. Fairbanks (1992), Evidence from Southern Ocean sediments for the effect of North Atlantic deep-water flux on climate, *Nature*, *355*, 416–419.

Chase, Z., R. F. Anderson, M. Q. Fleisher, and P. W. Kubik (2003), Accumulation of biogenic and lithogenic material in the Pacific sector of the Southern Ocean during the past 40,000 years, *Deep Sea Res., Part II*, *50*, 799–832.

Clark, P. U., N. G. Pisias, T. F. Stocker, and A. J. Weaver (2002), The role of the thermohaline circulation in abrupt climate change, *Nature*, *415*, 863–869.

CLIMAP (1976), The surface of the ice-age Earth, *Science*, *191*, 1131–1137.

Conkright, M., S. Levitus, and T. Boyer (1994), *World Ocean Atlas*, vol. 1, *Nutrients*, *NOAA Atlas NESDIS 1*, Natl. Oceanic and Atmos. Admin., Silver Spring, Md.

Cramer, W., et al. (2001), Global response of terrestrial ecosystem structure and function to CO_2 and climate change: results from six dynamic global vegetation models, *Global Change Biol.*, *7*, 357–375.

Crosta, X., and A. Shemesh (2002), Reconciling down core anticorrelation of diatom carbon and nitrogen isotopic ratios from the Southern Ocean, *Paleoceanography*, *17*(1), 1010, doi:10.1029/2000PA000565.

Crosta, X., J.-J. Pichon, and L. H. Burckle (1998a), Application of modern analog technique to marine Antarctic diatoms: Reconstruction of maximum sea-ice extent at the Last Glacial Maximum, *Paleoceanography*, *13*(3), 284–297.

Crosta, X., J.-J. Pichon, and L. H. Burckle (1998b), Reappraisal of Antarctic seasonal sea-ice extent at the Last Glacial Maximum, *Geophys. Res. Lett.*, *25*(14), 2703–2706.

Crowley, T. J (1983), Calcium-carbonate preservation patterns in the central North Atlantic during the last 150,000 years, *Mar. Geol.*, *51*, 1–14.

Curry, W. B., and G. P. Lohmann (1986), Late Quaternary carbonate sedimentation at the Sierra Leone rise (eastern equatorial Atlantic Ocean), *Mar. Geol.*, *70*, 223–250.

Curry, W. B., and D. W. Oppo (2005), Glacial water mass geometry and the distribution of $\delta^{13}C$ of ΣCO_2 in the western Atlantic Ocean, *Paleoceanography*, *20*, PA1017, doi:10.1029/2004PA001021.

Curry, W. B., J. C. Duplessy, L. D. Labeyrie, and N. J. Shackleton (1988), Changes in the distribution of $\delta^{13}C$ of deep water ΣCO_2 between the last glaciation and the Holocene, *Paleoceanography*, *3*(3), 317–341.

Delaygue, G., T. Stocker, F. Joos, and G.-K. Plattner (2003), Simulation of atmospheric radiocarbon during abrupt oceanic circulation changes: Trying to reconcile models and reconstructions, *Quat. Sci. Rev.*, *22*, 1647–1658.

Doney, S. C., et al. (2004), Evaluating global ocean carbon models: The importance of realistic physics, *Global Biogeochem. Cycles*, *18*, GB3017, doi:10.1029/2003GB002150.

Duplessy, J. C., N. J. Shackleton, R. G. Fairbanks, L. Labeyrie, D. Oppo, and N. Kallel (1988), Deep water source variations during the last climatic cycle and their impact on the global deepwater circulation, *Paleoceanography*, *3*(3), 343–360.

Emanuel, W. R., G. G. Killough, W. M. Post, and H. H. Shugart (1984), Modeling terrestrial ecosystems in the global carbon cycle with shifts in carbon storage capacity by land-use change, *Ecology*, *65*, 970–983.

Eyer, M. (2004), Highly resolved $\delta^{13}C$ measurements on CO_2 in air from Antarctic ice cores, Ph.D. thesis, Univ. of Bern, Bern, Switzerland.

Fairbanks, R. G. (1990), The age and origin of the Younger Dryas climate event in Greenland ice cores, *Paleoceanography*, *5*(6), 937–948.

Farrell, J. W., and W. L. Prell (1989), Climate change and $CaCO_3$ preservation: An 800,000 year bathymetric reconstruction from the central equatorial Pacific Ocean, *Paleoceanography*, *4*(4), 447–466.

Fichefet, T., B. Tartinville, and H. Goosse (2003), Antarctic sea ice variability during 1958–1999: A simulation with a global ice-ocean model, *J. Geophys. Res.*, *108*(C3), 3102, doi:10.1029/2001JC001148.

Fischer, H., M. Wahlen, J. Smith, D. Mastroianni, and B. Deck (1999), Ice core records of atmospheric CO_2 around the last three glacial terminations, *Science*, *283*, 1712–1714.

François, R., M. A. Altabet, E.-F. Yu, D. M. Sigman, M. P. Pacon, M. Frankl, G. Bohrmann, G. Bareille, and L. D. Labeyrie (1997), Contribution of Southern Ocean surface-water stratification to low atmospheric CO_2 concentrations during the last glacial period, *Nature*, *389*, 929–935.

Frank, M., R. Gersonde, M. R. van der Loeff, G. B. C. C. Nürnberg, P. M. Kubik, M. Suter, and A. Mangini (2000), Similar glacial and interglacial export bioproductivity in the Atlantic sector of the Southern Ocean: Multiproxy evidence and implications for glacial atmospheric CO_2, *Paleoceanography*, *15*(6), 642–658.

Ganachaud, A., and C. Wunsch (2000), Improved estimates of global ocean circulation, heat transport and mixing from hydrographic data, *Nature*, *408*, 453–457.

Gersonde, R., X. Crosta, A. Abelmann, and L. Armand (2005), Sea-surface temperature and sea ice distribution of the Southern Ocean at the EPILOG Last Glacial Maximum—A circum-Antarctic view based on siliceous microfossil records, *Quat. Sci. Rev.*, *24*, 869–896.

Gildor, H., E. Tziperman, and J. R. Toggweiler (2002), Sea ice switch mechanism and glacial-interglacial CO_2 variations, *Global Biogeochem. Cycles*, *16*(3), 1032, doi:10.1029/2001GB001446.

Gnanadesikan, A, R. D. Slater, N. Gruber, and J. L. Sarmiento (2002), Oceanic vertical exchange and new production: A comparison between models and observations, *Deep Sea Res., Part II*, *49*, 363–401.

Grootes, P. M., and M. Stuiver (1997), Oxygen 18/16 variability in Greenland snow and ice with 10^3 to 10^5-year time resolution, *J. Geophys. Res.*, *102*(C12), 26,455–26,470.

Guilderson, T. P., R. G. Fairbanks, and J. L. Rubenstone (2001), Tropical Atlantic coral oxygen isotopes: Glacial-interglacial sea surface temperature and climate change, *Mar. Geol.*, *172*, 75–89.

Harvey, L. D. D. (2001), A quasi-one-dimensional coupled climate-carbon cycle model: 2. The carbon cycle component, *J. Geophys. Res.*, *106*(C10), 22,355–22,372.

Heimann, M., and E. Maier-Reimer (1996), On the relations between the oceanic uptake of CO_2 and its carbon isotopes, *Global Biogeochem. Cycles*, *10*(1), 89–110.

Heimann, M., and P. Monfray (1989), Spatial and temporal variation of the gas exchange coefficient for CO_2: 1. Data analysis and global validation, *Rep. 31*, Max-Planck-Inst. for Meteorol., Hamburg, Germany.

Heinze, C., E. Maier-Reimer, and K. Winn (1991), Glacial pCO_2 reduction by the world ocean: Experiments with the Hamburg Carbon Cycle Model, *Paleoceanography*, *6*(4), 395–430.

Hemming, S. R. (2004), Heinrich events: Massive late Pleistocene detritus layers of the North Atlantic and their global climate imprint, *Rev. Geophys.*, *42*, RG1005, doi:10.1029/2003RG000128.

Hodell, D. A., C. D. Charles, J. H. Curtis, P. Graham Mortyn, U. S. Ninnemann, and K. A. Venz (2002), Data report: Oxygen isotope stratigraphy of ODP Leg 177 sites 1088, 1089, 1090, 1093, and 1094, in *Proceedings of the Ocean Drilling Program, Scientific Results*, vol. 177, edited by R. Gersonde, D. A. Hodell, and P. Blum, Table T2, Texas A&M, College Station, Texas. (Available online at http://wwwodp.tamu.edu/publications/177_SR/synth/synth.htm)

Hodell, D. A., K. A. Venz, C. D. Charles, and U. S. Ninnemann (2003), Pleistocene vertical carbon isotope and carbonate gradients in the South Atlantic sector of the Southern Ocean, *Geochem. Geophys. Geosyst.*, *4*(1), 1004, doi:10.1029/2002GC000367.

Howard, W. R, and W. L. Prell (1994), Late Quaternary $CaCO_3$ production and preservation in the Southern Ocean: Implications for oceanic and atmospheric carbon cycling, *Paleoceanography*, *9*(3), 453–482.

Hughen, K., S. Lehman, J. Southon, J. Overpeck, O. Marchal, C. Herring, and J. Turnbull (2004), ^{14}C activity and global carbon cycle changes over the past 50,000 years, *Science*, *303*, 202–207.

Ito, T., J. Marshall, and M. Follows (2004), What controls the uptake of transient tracers in the Southern Ocean?, *Global Biogeochem. Cycles*, *18*, GB2021, doi:10.1029/2003GB002103.

Joos, F., S. Gerber, I. C. Prentice, B. L. Otto-Bliesner, and P. J. Valdes (2004), Transient simulations of Holocenic atmospheric carbon dioxide and terrestrial carbon since the Last Glacial Maximum, *Global Biogeochem. Cycles*, *18*, GB2002, doi:10.1029/2003GB002156.

Jouzel, J., et al. (2001), A new 27 ky high resolution East Antarctic climate record, *Geophys. Res. Lett.*, *28*, 3199–3202.

Kageyama, M., O. Peyron, S. Pinot, P. Tarasov, J. Guiot, S. Jousaume, and G. Ramstein (2001), The Last Glacial Maximum climate over Europe and western Siberia: A PMIP comparsion between models and data, *Clim. Dyn.*, *17*, 23–43.

Kaplan, J. O., I. C. Prentice, W. Knorr, and P. J. Valdes (2002), Modeling the dynamics of terrestrial carbon storage since the Last Glacial Maximum, *Geophys. Res. Lett.*, *29*(22), 2074, doi:10.1029/2002GL015230.

Keir, R. S (1988), On the late Pleistocene ocean geochemistry and circulation, *Paleoceanography*, *3*(4), 413–445.

Key, R. M., A. Kozyr, C. L. Sabine, K. Lee, R. Wanninkhof, J. L. Bullister, R. A. Feely, F. J. Millero, C. Mordy, and T.-H. Peng (2004), A global ocean carbon climatology: Results from global data analysis project (GLODAP), *Global Biogeochem. Cycles*, *18*, GB4031, doi:10.1029/2004GB002247.

Kim, S.-J., G. M. Flato, G. J. Boer, and N. A. McFarlane (2002), A coupled climate model simulation of the Last Glacial Maximum: Part 1. Transient multi-decadal response, *Clim. Dyn.*, *19*, 515–537.

Klaas, C., and D. E. Archer (2002), Association of sinking organic matter with various types of mineral ballast in the deep sea: Implications for the rain ratio, *Global Biogeochem. Cycles*, *16*(4), 1116, doi:10.1029/2001GB001765.

Knorr, G, and G. Lohmann (2003), Southern Ocean origin for the resumption of Atlantic thermohaline circulation during deglaciation, *Nature*, *424*, 532–536.

Knox, F., and M. B. McElroy (1984), Changes in atmospheric CO_2: Influence of the marine biota at high latitude, *J. Geophys. Res.*, *89*(D3), 4629–4637.

Knutti, R., J. Flückiger, T. F. Stocker, and A. Timmermann (2004), Strong hemispheric coupling of glacial climate through continental freshwater discharge and ocean circulation, *Nature*, *430*, 851–856.

Koeve, W. (2002), Upper ocean carbon fluxes in the Atlantic Ocean: The importance of the POC:PIC ratio, *Global Biogeochem. Cycles*, *16*(4), 1056, doi:10.1029/2001GB001836.

Kohfeld, K. E, C. L. Quere, S. Harrison, and R. F. Anderson (2005), Role of marine biology in glacial-interglacial CO_2 cycles, *Science*, *308*, 74–78.

Köhler, P., and H. Fischer (2004), Simulating changes in the terrestrial biosphere during the last glacial/interglacial transition, *Global Planet. Change*, *43*(1–2), 33–55, doi:10.1016/j.gloplacha.2004.02.005.

Köhler, P., F. Joos, S. Gerber, and R. Knutti (2005), Simulated changes in vegetation distribution, land carbon storage, and atmospheric CO_2 in response to a collapse of the North Atlantic thermohaline circulation, *Clim. Dyn.*, *25*, 689–708, doi:10.1007/s00382-005-0058-8.

Körtzinger, A., J. I. Hedges, and P. D. Quay (2001), Redfield ratios revisited: Removing the biasing effect of anthropogenic CO_2, *Limnol. Oceanogr.*, *46*, 946–970.

Kroopnick, P. M. (1985), The distribution of ^{13}C of ΣCO_2 in the world oceans, *Deep Sea Res., Part A*, *32*, 57–84.

Kumar, N., R. F. Anderson, R. A. Mortlock, P. N. Froelich, P. Kubik, B. Dittrich-Hannen, and M. Suter (1995), Increased biological productivity and export production in the glacial Southern Ocean, *Nature*, *378*, 675–680.

Kutzbach, J., R. Gallimore, S. Harrison, P. Behling, R. Selin, and F. Laarif (1998), Climate and biome simulations for the past 21,000 years, *Quat. Sci. Rev.*, *17*, 473–506.

Labeyrie, L. D., J. C. Duplessy, and P. L. Blanc (1987), Variations in mode of formation and temperature of oceanic deep waters over the past 125,000 years, *Nature*, *327*, 477–482.

Laj, C., C. Kissel, A. Mazaud, E. Michel, R. Muscheler, and J. Beer (2002), Geomagnetic field intensity, North Atlantic Deep Water circulation and atmospheric $\Delta^{14}C$ during the last 50 kyr, *Earth Planet. Sci. Lett.*, *200*, 177–190.

Lea, D. W., D. K. Pak, and H. J. Spero (2000), Climate impact of late Quaternary equatorial Pacific sea surface temperature variations, *Science*, *289*, 1719–1724.

LeGrand, P., and K. Alverson (2001), Variations in atmospheric CO_2 during glacial cycles from an inverse ocean modelling perspective, *Paleoceanography*, *16*(6), 604–616.

Leuenberger, M. C., M. Eyer, P. Nyfeler, B. Stauffer, and T. F. Stocker (2003), High-resolution $\delta^{13}C$ measurements on ancient air extracted from less than 10 cm^3 of ice, *Tellus, Ser. B*, *55*, 138–144.

Levitus, S., and T. Boyer (1994a), *World Ocean Atlas*, vol. 2, *Oxygen*, NOAA Atlas NESDIS 2, Natl. Oceanic and Atmos. Admin., Silver Spring, Md.

Levitus, S., and T. Boyer (1994b), *World Ocean Atlas*, vol. 4, *Temperature*, NOAA Atlas NESDIS 4, Natl. Oceanic and Atmos. Admin., Silver Spring, Md.

Levitus, S., R. Burgett, and T. Boyer (1994), *World Ocean Atlas*, vol. 3, *Salinity, NOAA Atlas NESDIS 3*, Natl. Oceanic and Atmos. Admin., Silver Spring, Md.

Marchal, O., T. F. Stocker, and F. Joos (1998a), A latitude-depth, circulation-biogeochemical ocean model for paleoclimate studies: Development and sensitivities, *Tellus, Ser. B*, *50*, 290–316.

Marchal, O., T. F. Stocker, and F. Joos (1998b), Impact of oceanic reorganizations on the ocean carbon cycle and atmospheric carbon dioxide content, *Paleoceanography*, *13*(3), 225–244.

Marchal, O., T. F. Stocker, F. Joos, A. Indermühle, T. Blunier, and J. Tschumi (1999), Modelling the concentration of atmospheric CO_2 during the Younger Dryas climate event, *Clim. Dyn.*, *15*, 341–354.

Marchal, O., T. F. Stocker, and R. Muscheler (2001), Atmospheric radiocarbon during the Yonger Dryas: Production, ventilation, or both?, *Earth Planet. Sci. Lett.*, *185*, 383–395.

Martin, J. H. (1990), Glacial-interglacial CO_2 change: The iron hypothesis, *Paleoceanography*, *5*(1), 1–13.

Martin, P. A., D. W. Lea, Y. Rosenthal, N. J. Shackleton, M. Sarnthein, and T. Papenfuss (2002), Quaternary deep sea temperature histories derived from benthic foraminiferal Mg/Ca, *Earth Planet. Sci. Lett.*, *198*, 193–209.

Masarik, J., and J. Beer (1999), Simulation of particle fluxes of cosmogenic nuclide production in the Earth's atmosphere, *J. Geophys. Res.*, *104*(D10), 12,099–12,111.

Matsumoto, K., J. L. Sarmiento, and M. A. Brzezinski (2002), Silicic acid leakage from the Southern Ocean: A possible explanation for glacial atmospheric pCO_2, *Global Biogeochem. Cycles*, *16*(3), 1031, doi:10.1029/2001GB001442.

McManus, J. F, D. W. Oppo, and J. L. Cullen (1999), A 0.5-million-year record of millennial-scale climate variability in the North Atlantic, *Science*, *283*, 971–975.

McManus, J. F., R. Francois, J.-M. Gheradi, L. D. Keigwin, and S. Brown-Leger (2004), Collapse and rapid resumption of Atlantic meridional circulation linked to deglacial climate changes, *Nature*, *428*, 834–837.

McPhaden, M. J., and D. Zang (2002), Slowdown of the meridional overturning circulation in the upper Pacific Ocean, *Nature*, *415*, 603–608.

Meese, D. A., A. Gow, R. Alley, G. Zielinski, P. Grootes, M. Ram, K. Taylor, P. Mayewski, and J. Bolzan (1997), The Greenland Ice Sheet

Project 2 depth-age scale: Methods and results, *J. Geophys. Res.*, *102*(C12), 26,411–26,423.

Meissner, K. J., A. Schmittner, A. J. Weaver, and J. F. Adkins (2003), Ventilation of the North Atlantic Ocean during the Last Glacial Maximum: A comparison between simulated and observed radiocarbon ages, *Paleoceanography*, *18*(2), 1023, doi:10.1029/2002PA000762.

Millero, F. J, K. Lee, and M. Roche (1998), Distribution of alkalinity in the surface waters of the major oceans, *Mar. Chem.*, *60*, 111–130.

Milliman, J. D. (1993), Production and accumulation of calcium carbonate in the ocean: Budget of a nonsteady state, *Global Biogeochem. Cycles*, *7*(4), 927–957.

Mix, A. C., N. G. Pisias, R. Zahn, R. C. Lopez, and K. Nelson (1991), Carbon 13 in Pacific deep and inter mediate waters, 0–370 ka: Implications for ocean circulation and Pleistocene CO_2, *Paleoceanography*, *6*(2), 205–226.

Mix, A. C., J. Le, and N. J. Shackleton (1995), Benthic foraminiferal stable isotope stratigraphy of Site 846: 0–1.8 Ma, *Proc. Ocean Drill. Program Sci. Results*, *138*, 839–854.

Monnin, E., A. Indermühle, A. Dällenbach, J. Flückiger, B. Stauffer, T. F. Stocker, D. Raynaud, and J.-M. Barnola (2001), Atmospheric CO_2 concentrations over the last glacial termination, *Science*, *291*, 112–114.

Mook, W. G. (1986), ^{13}C in atmospheric CO_2, *Neth. J. Sea Res.*, *20*(2/3), 211–223.

Moore, J. K., M. R. Abbott, J. G. Richman, and D. M. Nelson (2000), The Southern Ocean at the Last Glacial Maximum: A strong sink for atmospheric carbon dioxide, *Global Biogeochem. Cycles*, *14*(1), 455–475.

Morales-Maqueda, M. A., and S. Rahmstorf (2002), Did Antarctic sea-ice expansion cause glacial CO_2 decline?, *Geophys. Res. Lett.*, *29*(1), 1011, doi:10.1029/2001GL013240.

Mulitza, S., H. Arz, S. K. von Mücke, C. Moss, H. S. Niebler, J. Pätzold, and M. Segl (1999), The South Atlantic Carbon Isotope record of planktic foraminifera, in *Use of Proxies in Paleoceanography: Examples From the South Atlantic*, edited by G. Fischer and G. Wefer, pp. 427–445, Springer, New York.

Munhoven, G. (1997), Modelling glacial-interglacial atmospheric CO_2 variations: The role of continental weathering, Ph.D. thesis, Univ. de Liège, Liège, Belgium.

Munhoven, G (2002), Glacial-interglacial changes of continental weathering: estimates of the related CO_2 and HCO_3^- flux variations and their uncertainties, *Global Planet. Change*, *33*, 155–176.

Munhoven, G., and L. M. François (1996), Glacial-interglacial variability of atmospheric CO_2 due to changing continental silicate rock weathering: A model study, *J. Geophys. Res.*, *101*(D16), 21,423–21,437.

Muscheler, R., J. Beer, G. Wagner, C. Laj, C. Kissel, G. M. Raisbeck, F. Yiou, and P. W. Kubik (2004), Changes in the carbon cycle during the last deglaciation as indicated by the comparison of ^{10}Be and ^{14}C records, *Earth Planet. Sci. Lett.*, *219*, 325–340.

Nürnberg, D., A. Müller, and R. R. Schneider (2000), Paleo-sea surface temperature calculations in the equatorial east Atlantic from Mg/Ca ratios in planktic foraminifera: A comparison to sea surface temperature estimates from $U_{37}^{K'}$, oxygen isotopes, and foraminiferal transfer function, *Paleoceanography*, *15*(1), 124–134.

Opdyke, B. N., and J. C. G. Walker (1992), Return of the coral reef hypothesis: Basin to shelf partitioning of $CaCO_3$ and its effect on atmospheric CO_2, *Geology*, *20*, 733–736.

Oppo, D. W., and S. J. Lehman (1993), Mid-depth circulation of the subpolar North Atlantic during the Last Glacial Maximum, *Science*, *259*, 1148–1152.

Paillard, D., and F. Parrenin (2004), The Antarctic ice sheet and the triggering of deglaciations, *Earth Planet. Sci. Lett.*, *227*, 263–271.

Passow, U. (2004), Switching perspectives: Do mineral fluxes determine particulate organic carbon fluxes or vice versa?, *Geochem. Geophys. Geosyst.*, *5*, Q04002, doi:10.1029/2003GC000670.

Peterson, L. C., and W. L. Prell (1985), Carbonate preservation and rates of climate change: An 800 kyr record from the Indian Ocean, in *The Carbon Cycle and Atmospheric CO_2: Natural Variations Archean to Present*, *Geophys. Monogr. Ser.*, vol. 32, edited by E. T. Sundquist and W. S. Broecker, pp. 251–269, AGU, Washington, D. C.

Pflaumann, U., et al. (2003), Glacial North Atlantic: Sea-surface conditions reconstructed by GLAMAP2000, *Paleoceanography*, *18*(3), 1065, doi:10.1029/2002PA000774.

Prieto, F. J. M, and F. J. Millero (2002), The values of $pK_1 + pK_2$ for the dissolution of carbonic acid in seawater, *Geochim. Cosmochim. Acta*, *66*, 2529–2540.

Qiu, B., and R. Huang (1995), Ventilation of the North Atlantic and North Pacific: Subduction versus obduction, *J. Phys. Oceanogr.*, *25*, 2374–2390.

Rahmstorf, S. (2002), Ocean circulation and climate during the past 120,000 years, *Nature*, *419*, 207–214.

Rau, G. H., U. Riebesell, and D. Wolf-Gladrow (1996), A model of photosynthetic ^{13}C fractionation by marine phytoplankton based on diffusive molecular CO_2 uptake, *Mar. Ecol. Prog. Ser.*, *133*, 275–285.

Rau, G. H., U. Riebesell, and D. Wolf-Gladrow (1997), CO_{2aq}-dependent photosynthetic ^{13}C fractionation in the ocean: A model versus measurements, *Global Biogeochem. Cycles*, *11*(2), 267–278.

Ridgwell, A. J. (2001), Glacial-interglacial pertubations in the global carbon cycle, Ph.D. thesis, Univ. of East Anglia, Norwich, UK.

Ridgwell, A. J. (2003a), An end to the rain ratio reign?, *Geochem. Geophys. Geosyst.*, *4*(6), 1051, doi:10.1029/2003GC000512.

Ridgwell, A. J. (2003b), Implications of the glacial CO_2 iron hypothesis for Quaternary climate change, *Geochem. Geophys. Geosyst.*, *4*(9), 1076, doi:10.1029/2003GC000563.

Ridgwell, A. J., and A. J. Watson (2002), Feedback between aeolian dust, climate, and atmospheric CO_2 in glacial time, *Paleoceanography*, *17*(4), 1059, doi:10.1029/2001PA000729.

Robinson, R. S., B. G. Brunelle, and D. M. Sigman (2004), Revisiting nutrient utilization in the glacial Antarctic: Evidence from a new method for diatom-bound N isotopic analysis, *Paleoceanography*, *19*, PA3001, doi:10.1029/2003PA000996.

Röthlisberger, R., R. Mulvaney, E. W. Wolff, M. A. Hutterli, M. Bigler, S. Sommer, and J. Jouzel (2002), Dust and sea salt variability in central East Antarctica (Dome C) over the last 45 kyrs and its implications for southern high-latitude climate, *Geophys. Res. Lett.*, *29*(20), 1963, doi:10.1029/2002GL015186.

Röthlisberger, R., M. Bigler, E. W. Wolff, E. Monnin, F. Joos, and M. Hutterli (2004), Ice core evidence for the extent of past atmospheric CO_2 change due to iron fertilization, *Geophys. Res. Lett.*, *31*, L16207, doi:10.1029/2004GL020338.

Saltzman, J, and K. F. Wishner (1997), Zooplankton ecology in the eastern tropical Pacific oxygen minimum zone above a seamount: 1. General trend, *Deep Sea Res., Part I*, *44*, 907–930.

Sarmiento, J. L., and J. R. Toggweiler (1984), A new model for the role of the oceans in determining atmospheric P_{CO_2}, *Nature*, *308*, 621–624.

Sarmiento, J. L., J. C. Orr, and U. Siegenthaler (1992), A pertubation simulation of CO_2 uptake in an ocean general circulation model, *J. Geophys. Res.*, *97*(C3), 3621–3645.

Sarmiento, J. L., J. Dunne, A. Gnanadesikan, R. M. Key, K. Matsumoto, and R. Slater (2002), A new estimate of the $CaCO_3$ to organic carbon export ratio, *Global Biogeochem. Cycles*, *16*(4), 1107, doi:10.1029/2002GB001919.

Sarnthein, M., U. Pflaumann, and M. Weinelt (2003), Past extent of sea ice in the northern North Atlantic inferred from foraminiferal paleotemperature estimates, *Paleoceanography*, *18*(2), 1047, doi:10.1029/2002PA000771.

Schiebel, R. (2002), Planktic foraminiferal sedimentation and the marine calcite budget, *Global Biogeochem. Cycles*, *16*(4), 1065, doi:10.1029/2001GB001459.

Schlitzer, R. (2000), Applying the adjoint method for biogeochemical modelling: Export of particulate organic matter in the world ocean, in *Inverse Methods in Global Biogeochemical Cycles*, *Geophys. Monogr. Ser.*, vol. 114, edited by P. Kasibhatla et al., pp. 107–124, AGU, Washington, D. C.

Schlitzer, R (2002), Carbon export fluxes in the Southern Ocean: Results from inverse modeling and comparison with satellite-based estimates, *Deep Sea Res., Part II*, *49*, 1623–1644.

Scholze, M., W. Knorr, and M. Heimann (2003), Modelling terrestrial vegetation dynamics and carbon cycling for an abrupt climate change event, *Holocene*, *13*, 327–333.

Schulz, M., D. Seidov, M. Sarnthein, and K. Stattegger (2001), Modelling ocean-atmosphere carbon budgets during the Last Glacial Maximum—Heinrich 1 meltwater event—Bølling transition, *Int. J. Earth Sci.*, *90*, 412–425.

Siegenthaler, U., and T. Wenk (1984), Rapid atmospheric CO_2 variations and ocean circulation, *Nature*, *308*, 624–626.

Sigman, D. M., and E. A. Boyle (2000), Glacial/interglacial variations in atmospheric carbon dioxide, *Nature*, *407*, 859–869.

Sigman, D. M., D. C. McCorkle, and W. R. Martin (1998), The calcite lysocline as a constraint on glacial/interglacial low-latitude production changes, *Global Biogeochem. Cycles*, *12*(3), 409–427.

Slowey, N. C., and W. B. Curry (1995), Glacial-interglacial differences in circulation and carbon cycling within the upper western North Atlantic, *Paleoceanography*, *10*(4), 715–732.

Sloyan, B. M., and S. R. Rintoul (2001), The Southern Ocean limb of the global deep overturning circulation, *J. Phys. Oceanogr.*, *31*, 143–173.

Smith, H. J., H. Fischer, M. Wahlen, D. Mastroianni, and B. Deck (1999), Dual modes of the carbon cycle since the Last Glacial Maximum, *Nature*, *400*, 248–250.

Spero, H. J., and D. W. Lea (2002), The cause of carbon isotope minimum events on glacial terminations, *Science*, *296*, 522–525.

Spero, H. J., J. Bijma, D. W. Lea, and B. E. Bemis (1997), Effect of seawater carbonate concentration on foraminiferal carbon and oxygen isotopes, *Nature*, *390*, 497–500.

Stenni, B., V. Masson-Delmotte, S. Johnsen, J. Jouzel, A. Longinelli, E. Monnin, R. Röthlisberger, and E. Selmo (2001), An oceanic cold reversal during the last deglaciation, *Science*, *293*, 2074–2077.

Stephens, B. B., and R. F. Keeling (2000), The influence of Antarctic sea ice on glacial-interglacial CO_2 variations, *Nature*, *404*, 171–174.

Stocker, T. F., and D. G. Wright (1996), Rapid changes in ocean circulation and atmospheric radiocarbon, *Paleoceanography*, *11*(6), 773–795.

Stuiver, M., H. G. Östlund, and T. A. McConnaughey (1981), GEOSECS Atlantic and Pacific ^{14}C distribution, in *Carbon Cycle Modelling*, *Sci. Comm. Problems Environ. (SCOPE) Ser.*, vol. 16, edited by B. Bolin, pp. 201–221, John Wiley, Hoboken, N. J.

Stuiver, M., P. J. Reimer, E. Bard, J. W. Beck, G. S. Burr, K. A. Hughen, B. Kromer, G. McCormac, J. van der Plicht, and M. Spurk (1998), INTCAL98 radiocarbon age calibration, 24,000-0 cal BP, *Radiocarbon*, *40*, 1041–1083.

Takahashi, T., W. S. Broecker, and A. E. Bainbridge (1981), The alkalinity and total carbon dioxide concentration in the world oceans, in *Carbon Cycle Modelling*, *Sci. Comm. Problems Environ. (SCOPE) Ser.*, vol. 16, edited by B. Bolin, pp. 271–286, John Wiley, Hoboken, N. J.

Takahashi, T., et al. (2002), Global sea-air CO_2 flux based on climatological surface ocean $p CO_2$, and seasonal biological and temperature effects, *Deep Sea Res., Part II*, *49*, 1601–1622.

Toggweiler, J. R. (1999), Variation of atmospheric CO_2 by ventilation of the ocean's deepest water, *Paleoceanography*, *14*(5), 571–588.

Toggweiler, J. R., and J. L. Sarmiento (1985), Glacial to interglacial changes in atmospheric carbon dioxide: The critical role of ocean surface water in high latitudes, in *The Carbon Cycle and Atmospheric CO_2: Natural Variations Archean to Present*, *Geophys. Monogr. Ser.*, vol. 32, edited by E. T. Sundquist and W. S. Broecker, pp. 163–184, AGU, Washington, D. C.

Toggweiler, J. R., A. Gnanadesikan, S. Carson, R. Murnane, and J. L. Sarmiento (2003a), Representation of the carbon cycle in box models and GCMs: 1. Solubility pump, *Global Biogeochem. Cycles*, *17*(1), 1026, doi:10.1029/2001GB001401.

Toggweiler, J. R., R. Murnane, S. Carson, A. Gnanadesikan, and J. L. Sarmiento (2003b), Representation of the carbon cycle in box models and GCMs: 2. Organic pump, *Global Biogeochem. Cycles*, *17*(1), 1027, doi:10.1029/2001GB001841.

Vecsei, A (2004), Carbonate production on isolated banks since 20 k.a. BP: Climatic implications, *Palaeogeogr. Palaeoclimatol. Palaeoecol.*, *214*, 3–10.

Vecsei, A., and W. H. Berger (2004), Increase of atmospheric CO_2 during deglaciation: Constraints on the coral reef hypothesis from patterns of deposition, *Global Biogeochem. Cycles*, *18*, GB1035, doi:10.1029/2003GB002147.

Vinnikov, K. Y., A. Robock, R. J. Stouffer, J. E. Walsh, C. L. Parkinson, D. J. Cavalieri, J. F. B. Mitchell, D. Garrett, and V. F. Zakharov (1999), Global warming and Northern Hemisphere sea ice extent, *Science*, *286*, 1934–1937.

Visser, K., R. Thunell, and L. Stott (2003), Magnitude and timing of temperature change in the Indo-Pacific warm pool during deglaciation, *Nature*, *421*, 152–155.

Wanninkhof, R. (1992), Relationship between wind speed and gas exchange over the ocean, *J. Geophys. Res.*, *97*(C5), 7373–7382.

Watson, A. J., D. C. E. Bakker, A. J. Ridgwell, P. W. Boyd, and C. S. Law (2000), Effect of iron supply on Southern Ocean CO_2 uptake and implications for glacial atmospheric CO_2, *Nature*, *407*, 730–733.

Winguth, A. M. E., D. Archer, J.-C. Duplessy, E. Maier-Reimer, and U. Mikolajewicz (1999), Sensitivity of paleonutrient tracer distributions and deep-sea circulation to glacial boundary conditions, *Paleoceanography*, *14*(3), 304–323.

Wunsch, C. (1984), An estimate of the upwelling rate in the equatorial Atlantic based on the distribution of bomb radiocarbon and quasigeostrophic dynamics, *J. Geophys. Res.*, *89*(C5), 7971–7978.

Zeebe, R. E., and P. Westbroek (2003), A simple model for the $CaCO_3$ saturation state of the ocean: The Strangelove, the Neritan, and the Cretan Ocean, *Geochem. Geophys. Geosyst.*, *4*(12), 1104, doi:10.1029/2003GC000538.

Zeebe, R. E., and D. A. Wolf-Gladrow (2001), *CO_2 in Seawater: Equilibrium, Kinetics, Isotopes*, *Oceanogr. Book Ser.*, vol. 65, 346 pp., Elsevier, New York.

Zhang, J, P. D. Quay, and D. O. Wilbur (1995), Carbon isotope fractionation during gas-water exchange and dissolution of CO_2, *Geochim. Cosmochim. Acta*, *59*, 107–114.

————————————

H. Fischer and P. Köhler, Alfred Wegener Institute for Polar and Marine Research, P.O. Box 12 01 61, D-27515 Bremerhaven, Germany. (pkoehler@awi-bremerhaven.de)

G. Munhoven, Laboratoire de Physique Atmosphérique et Planétaire, Institut d'Astrophysique et de Géophysique, Université de Liège, 5 avenue de Cointe, B-4000 Liège, Belgium.

R. E. Zeebe, Department of Oceanography, University of Hawaii at Manoa, 1000 Pope Road, Marine Sciences Building, Honolulu, HI 96822, USA.